Neoplasma 2025; 72(4): 286–299

doi:10.4149/neo_2025_250321N133

High glycolysis phenotype influences malignant progression and poor prognosis of gastric cancer through the PI3K/AKT pathway

Shiya LIU[1,#], Gaigai SHEN[1,#], Xuanyu ZHOU[2], Guanghui WANG[3], Huiqi LIU[3], Yuanting CAO[1], Lixin SUN[1,*], Xiong SHU[4,*], Yuliang RAN[1,*]

[1]State Key Laboratory of Molecular Oncology, National Cancer Center/National Clinical Research Center for Cancer/Cancer Hospital, Chinese Academy of Medical Sciences and Peking Union Medical College, Chaoyang, Beijing, China; [2]Department of Epidemiology and Population Health, Stanford University of Medicine, Stanford, California, United States; [3]Department of Basic Medical Sciences, Medical College of Qinghai University, Xining, Qinghai, China; [4]Beijing Research Institute of Orthopaedics and Traumatology, Beijing Jishuitan Hospital, Capital Medical University, Xicheng, Beijing, China

**Correspondence: sunlixinslx@aliyun.com; shuxiong@jst-hosp.com.cn; ranyuliang@cicams.ac.cn*
#Contributed equally to this work.

Received March 21, 2025 / Accepted July 10, 2025

Gastric cancer (GC) is a prevalent gastrointestinal malignancy, with metabolic reprogramming, particularly glycolysis, playing a critical role in cancer cell stemness. However, the interaction between glycolysis and GC prognosis, along with its underlying mechanisms, remains poorly understood. This study aimed to systematically analyze the prognostic significance of glycolysis in GC and explore its functional impact. A glycolysis-related gene score was constructed using bioinformatics to assess glycolysis levels based on differentially expressed genes between GC and normal tissues. A nomogram model was developed to predict clinical prognosis, and the functional phenotypes of GC cell lines cultured under high and low glucose conditions were evaluated using metabolite detection and extracellular acidification rate (ECAR) measurements. Enrichment analyses identified key signaling pathways, which were further validated by western blot. Results showed that elevated glycolysis was associated with larger tumor size and poorer prognosis in GC patients. The nomogram demonstrated strong predictive accuracy. High glucose culture promoted glucose consumption, lactate production, ATP generation, and ECAR, enhancing epithelial-mesenchymal transition and malignant progression via the PI3K/AKT pathway. In conclusion, high glycolysis is linked to poor prognosis in GC and drives metastasis and stemness through the PI3K/AKT signaling pathway, highlighting its potential as a prognostic marker and therapeutic target.

Key words: gastric cancer; glycolysis; prognostic; hyperglycemia; PI3K/AKT

Gastric cancer (GC) is the fifth most common malignancy and the fourth leading cause of cancer-related mortality [1, 2]. Despite the decreased global incidence of GC [3], it remains highest in East Asian countries, including China [4]. The efficacy of traditional clinical treatments for GC, including surgery and chemoradiotherapy, is limited, resulting in poor patient prognoses and stagnant five-year survival rates. The primary reasons for the limited efficacy include the complex GC driver genes, high intra-tumor and inter-tumor heterogeneity, and the presence of cancer stem cells (CSCs). CSCs, in particular, contribute to metastasis, recurrence, and drug resistance [5]. Metabolism plays a crucial role in GC and impacts patient prognosis [6]. Epithelial-mesenchymal transition (EMT) represents a reversible cellular program that may serve as a pivotal early stage of tumor metastasis [7]. Furthermore, hyperglycemia promotes cell invasion and metastasis in various cancers [8]. However, the mechanisms underlying this phenomenon remain unclear.

Metabolic reprogramming, an emerging hallmark of cancer [9], has gained substantial attention in the last few years. The relationship between metabolic reprogramming and cancer has been extensively validated, and glycolysis is a crucial pathway for energy metabolism reprogramming in tumor cells. Tumor cells exhibit significantly elevated glycolysis levels, preferentially utilizing this pathway for energy production under both hypoxic and aerobic environments [10]. Metabolic reprogramming has been observed *in vivo* in various tumor types and is closely associated with the maintenance of CSCs, cancer progression, metastasis, and drug resistance [11]. Metabolism, particularly glycolysis, is intricately linked with EMT and stemness in tumor cells [12, 13]. Alterations in glycolysis levels in tumor cells are

associated with stemness-associated characteristics exhibited by the entire tumor cell population [14]. Under normal circumstances, cells are not affected by any changes in intracellular glucose metabolism due to changes in blood sugar in the body. However, tumor cells are highly sensitive to fluctuations in glucose concentration in the external environment, thereby regulating intracellular glucose metabolism and changing their metabolic mode to ensure survival and further metastasis and proliferation. However, the regulation of glycolysis in tumor cells and its role in controlling EMT and metastasis remain unclear.

Consequently, we investigated the effects of elevated glucose levels on EMT and stemness in tumors. In this study, the effects of high glucose levels on GC cell metastasis and stemness were evaluated using both clinical data and biological experiments. Furthermore, the objective of this study was to gain preliminary insight into the molecular mechanisms through which high glucose exerts these effects. Our results have significant clinical implications for identifying specific targets and inhibitors related to tumor metabolism and stemness [11]. Thus, our findings provide valuable insights into GC that may contribute to developing new therapeutic strategies.

Materials and methods

Cell lines and culture. The human GC cell lines MGC803 and HGC27 were obtained from the Chinese Academy of Sciences (China). The cells were cultured in DMEM complete media containing 10% fetal bovine serum, 1% L-glutamine, penicillin, and streptomycin. All cells were cultured in a 37 °C incubator with 5% CO_2.

Data processing and establishment of the glycolysis-related gene (GRG) score model. Gene expression data were extracted from The Cancer Genome Atlas (TCGA) database. The "limma" package was used to select differentially expressed genes (DEGs) between the tumor and normal tissues with the following criteria: FDR-adjusted p-values <0.05 and |fold change| >1.5. The Molecular Signatures Database (MSigDB) v4.0 was searched for glycolysis-related gene sets (HALLMARK_GLYCOLYSIS). Gene set enrichment analysis (GSEA) was performed on DEGs to identify pathways and networks potentially involved in GC progression. From the 4,266 DEGs, 54 GRGs were identified using a Venn diagram. Next, Cox regression analysis and Least Absolute Shrinkage and Selection Operator (LASSO) regression were performed to identify glycolytic target genes associated with overall survival (OS) to establish the GRG score model. The GRG scores for patients with stomach adenocarcinoma (STAD) were calculated based on the coefficients (Coefi) and expression levels (Expri) of the prospective prognostic GRGs using the following formula: GRG score = $\sum_{i=1}^{n}$Coefi × Expri.

Construction and evaluation of the GRG prognostic model. Data from TCGA database were used as the training set. The median GRG score (median=0.033) was used as the cutoff to divide 355 TCGA-STAD patients into the high and low glycolysis groups. Kaplan-Meier curves were plotted to compare the OS between the high and low GRG score groups. Time-dependent receiver operating characteristic (ROC) curves were used to evaluate the predictive ability of the GRG score model. To validate the prognostic model, the same process was carried out on a testing dataset from the Gene Expression Omnibus (GEO) (GSE62254, N=300).

Development of a nomogram based on GRG scores and clinical factors in TCGA-STAD. The "compare Groups" R package was used to compare the predictive efficacy of the GRG score with clinical characteristics. Cox regression analysis was applied to evaluate the independent prognostic value of the GRG scores and other clinical features. A nomogram was constructed using the R package "rms" and "regplot" to predict prognosis, based on GRG scores and clinical features. Calibration plots of the nomograms were created to assess the predictive accuracy of the nomogram using the "caret" package. ROC curves were used to validate the predictive ability of the nomogram.

GRG score model differential analysis and enrichment analysis. The TCGA-STAD dataset was divided into 2 groups based on the median glycolysis score. DEGs were selected using the following criteria: FDR-adjusted p-values < 0.05 and |fold change| >1.5 between the high and low GRG score group. The differential biological effects and signaling pathways between the high and low glycolysis groups in the gene ontology (GO) and Kyoto Encyclopedia of Genes and Genomes (KEGG) databases were evaluated using the "cluster Profiler" package in R. GSEA was employed to assess whether expressions of specific gene sets from the MSigDB collection (h.all.v2023.1.Hs.symbols.gmt) were significantly different between the high and low glycolysis groups.

Calculation of EMT and stemness scores. The pan-cancer 78-gene EMT signature was downloaded from the EMTome online database (https://www.emtome.org/) [15]. The expression levels of the 78 genes were calculated as the sum across all samples. The top 10 mesenchymal genes (MGene_top10) and the top 10 epithelial genes (EGene_top10) were defined. The EMT score for each sample (panCancer_EMTscore) was calculated as the difference in expression values between the MGene_top10 and EGene_top10. A higher EMT score indicates a more mesenchymal phenotype and a less epithelial phenotype. The stemness score (ssGSVA score) was constructed with the "GSVA" R package using 109 cancer stem cell-related genes compiled from previous research [16].

Glucose consumption and lactate production measurement. Cells were seeded into 6-well plates. After 24 h, 2 ml of fresh medium was used instead. Following a fixed incubation period, the cell culture supernatant was collected. Glucose consumption was assessed using a colorimetric method according to the instructions of the Glucose and Sucrose Assay Kit (Sigma-Aldrich, #MAK013, USA). Lactate production was measured using the Lactate Assay Kit II (Abcam,

#ab65331, UK). Glucose consumption and lactate production were normalized to the number of cells (μmol/10^6 cells).

Adenosine 5'-triphosphate (ATP) production measurement. Cells were seeded into 6-well plates. After 24 h, 2 ml of fresh medium was used instead. Following a fixed incubation period, the cells were collected, and ATP production was measured using the ATP Assay Kit (Beyotime, #S0027, China). ATP production was normalized to the control group (nmol/mg protein).

Extracellular acidification rate (ECAR) measurement. Cells were seeded in XF96 plates (15,000 cells/well) and incubated overnight. After washing, the cells were incubated in a 37 °C CO_2-free incubator for 60 min. Glucose (10 mM), oligomycin (1 μM), and 2-deoxyglucose (2-DG, 50 mM) were added, and ECAR was measured at the specified time points. The ECAR was assessed using the Seahorse XFe96 analyzer (Agilent Technologies Inc., USA) to evaluate glycolytic flux.

Oxygen consumption rate (OCR) measurement. Cells were seeded in XF96 plates (15,000 cells/well) and incubated overnight. After washing, the cells were incubated in a 37 °C CO_2-free incubator for 60 min. Oligomycin (1 μM), carbonyl cyanide 4-(trifluoromethoxy) phenylhydrazone (FCCP, 1 μM), and rotenone/antimycin A (0.5 μM) were sequentially added, and OCR was measured at the specified time points. OCR was determined using the Seahorse XFe96 analyzer (Agilent Technologies Inc., USA) to assess mitochondrial respiration.

Cell invasion and migration assay. To assess cell migration and invasion, Transwell™ chambers (24-well inserts; pore size, 8 μm; Corning, USA) were either left uncoated or coated with diluted Matrigel (BD Biosciences, USA). Serum-starved cells (2×10^4) were seeded in the upper chamber with serum-free medium, while the lower chamber contained complete medium with varying glucose concentrations. After 24 h of incubation at 37 °C, the cells that had migrated through the membrane were fixed, stained, photographed, and counted. Quantitative analysis was then performed to assess cell migration and invasion.

Cell proliferation analysis. Cells cultured in high- and low-glucose environments were seeded in 96-well plates (approximately 5,000 cells/well) and cultured in media with different glucose concentrations. Using the IncuCyte S3 platform (Sartorius, Göttingen, Germany), phase contrast images were collected from two regions within each well at 3 h intervals using a 10× objective. The IncuCyte S3 image analysis software was set to detect cell edges and determine their confluence percentage. Proliferation curves were plotted based on the confluence percentage over time to evaluate cell proliferation capacity.

Sphere formation assay. A solution of 0.8% methylcellulose was prepared [14], and 2 ml of the solution was added to each well of a low-adhesion 24-well plate. Cells were cultured in high- and low-glucose environments during their logarithmic growth phase and harvested. The cell density was adjusted to 5×10^4 cells/ml, and 10 μl of the cell suspension was added to the methylcellulose in each well. Cells were incubated at 37 °C with 5% CO_2 for 7–14 days. Photograph and count the number and size of spheres under an inverted fluorescence microscope.

Colony formation assay. Cells are cultured in high- and low-glucose environments during their logarithmic growth phase. The cell density was adjusted to 5×10^3 cells/ml, and 20 μl of the cell suspension was added to each well of a 6-well plate and gently shaken to disperse the cells. Every 3 days, 1 ml of the corresponding fresh medium was added. Cells were incubated at 37 °C until visible colonies formed. The colonies were fixed with 2 ml of 4% formaldehyde (Solarbio, China) for 30 min, stained with 2 ml of 0.1% crystal violet (Solarbio, China) for 30 min, rinsed with PBS, air dried, and photographed. Count the number of colonies formed in each group.

Protein extraction and western blot. Cells cultured in high- and low-glucose environments were lysed to extract total protein. The proteins were separated using SDS-PAGE and transferred to membranes, followed by the addition of ECL detection reagent for visualization. Western blot band grayscale values were quantified using ImageJ software. Target protein band densities were normalized to the corresponding β-actin internal control.

The following primary antibodies were used: CD44 (#ab157107), SOX2 (#ab97959), and Oct4 (#ab18976), were from Abcam (USA), and vimentin (#5741S), β-actin (#4970S), E-cadherin (#3195S), N-cadherin (#13116S), Snail (#3879S), Nanog (#3580S), p-PI3K (#4228S), PI3K (#4249S), p-AKT (#4060S) and AKT (#2920S) were from Cell Signaling Technology (USA). Secondary antibodies were HRP-labeled goat anti-rabbit and anti-mouse IgG (Jackson, USA).

Statistical analysis. Statistical analysis and data visualization were performed using R version 4.2.0, SPSS 25.0, and GraphPad Prism 8.0. All experiments were repeated three times, and the data are presented as means ± standard deviation ($\bar{x}\pm s$). Normality and homogeneity of variance analyses were conducted on the data. A p-value <0.05 was considered statistically significant.

Results

Impact of the high glycolysis model on prognosis in patients with GC. Using TCGA data, we identified DEGs between GC and normal tissues (Supplementary Figure S1A). Based on the glycolysis gene set from the hallmark database, glycolysis genes were significantly enriched in GC patients (Supplementary Figure S1B). After integrating DEGs from TCGA, we selected 54 glycolysis-related DEGs in tumor tissues versus normal tissues for further study (Supplementary Figure S1C). After filtering through LASSO and multivariable Cox regression analysis (Supplementary Figures S1D, S1E), 4 genes (STC1, VCAN, SOX9, and AK4) significantly associated with OS were identified ($p<0.05$). GRG scores were calculated using the following formula:

GRG score = (0.1908 × STC1) + (0.1034 × VCAN) + (−0.1660 × SOX9) + (0.1216 × AK4). STAD patients were divided into the high and low glycolysis groups based on the GRG scores. The heatmap displays the expression profiles of the four genes. Compared to the low glycolysis group, the expression levels of AK4, STC1, and VCAN were higher in the high glycolysis group, whereas SOX9 expression was lower in the high glycolysis group (Figure 1A).

The relationship between the survival status and time of GC patients was ranked by GRG scores (Figure 1B). Based on the Kaplan-Meier survival analysis, the predictive model exhibited strong prognostic capability, with the low glycolysis group showing a higher survival rate and patients in the high glycolysis group showing shorter survival times ($p<0.005$; Figure 1C). The predictive ability of the prognostic model was validated using the 1-year, 3-year, and 5-year ROC curves; the AUC values of the ROC curves were all above 0.6, indicating that the GRG score model accurately predicted prognosis in patients with GC (Figure 1D).

The ACGR cohort (GSE62254, N=300) from the GEO database was selected as the testing gene set to verify the GRG scoring model using the same methodology. The distribution of the four GRG-related genes in the heatmap plot (Figure 1E) and the survival status stratified by median GRG scores (median=0.411; Figure 1F) were similar to the previous findings. The Kaplan-Meier survival curves demonstrated that the survival rate of the low glycolysis group was higher than the survival rate of the high glycolysis group (Figure 1G), consistent with the results from the TCGA-STAD. Additionally, the GRG score-based model exhibited good sensitivity and specificity, with AUC values above 0.6 in ROC curves (Figure 1H). Further analysis of the relationship between the GRG score and clinical pathological characteristics revealed that high glycolysis levels were associated with larger tumor size in patients with GC (Supplementary Table S1, Supplementary Figure S2A). Meanwhile, TCGA project has classified GC into four molecular subtypes, including genome stable (GS), MSI, EBV, and chromosomal instability (CIN). We found that the distribution of the GRG score varies significantly among different molecular subtypes, and higher GRG score cases were concentrated in the subtypes of GS (Supplementary Figures S2B, S2C).

Nomogram for predicting prognosis in GC patients combining glycolysis and clinical characteristics. A glycolysis-clinical nomogram was developed to predict individual survival rates based on glycolysis and clinical factors. First, Cox regression analyses were conducted to evaluate the GRG score and other clinical features. The univariate Cox results indicated that age, stage, tumor node metastasis (TNM) classification, and the GRG score were associated with OS (Figure 2A). More total points were associated with shorter 1-year, 3-year, and 5-year survival times (Figure 2B). Multivariate regression revealed only 3 independent prognostic factors (Supplementary Table S1). Calibration curves comparing the predicted survival times with observed 1-year, 3-year, and 5-year survival times (Figure 2C) indicated that the nomogram prediction model accurately predicted the survival time of patients with GC within a 5-year period.

The GRG score model exhibited better predictive accuracy compared to clinical features such as tumor grade and TNM classification. The nomogram model combining the GRG score with significant clinical features from the multivariate Cox analysis exhibited the highest AUC (>0.7) (Figure 2D). Thus, combining glycolysis and clinical factors reliably predicted patient prognosis, highlighting the clinical significance of glycolysis.

High and low glucose culture environments induce different glycolytic phenotypes in GC cells. To verify the impact of glycolysis on the malignant GC phenotype, MGC803 and HGC27 GC cell lines were cultured in media with 25 mM, 15 mM, and 5.5 mM glucose to establish cell lines with varying glycolytic phenotypes. Treatment with different glucose concentrations significantly altered the glycolytic levels in GC cells. A high-glucose environment significantly increased glucose consumption and the production of major glycolytic products, including lactate and ATP (Figures 3A–3C). High-glucose culture also significantly elevated the ECAR levels in GC cells (Figure 3D). Conversely, a low-glucose environment significantly reduced glucose consumption, lactate production, ATP generation, and ECAR in GC cells. We further performed mitochondrial OCR assays in MGC803 and HGC27 cells. The results demonstrated that neither basal respiration, maximal respiratory capacity, nor ATP-linked respiration showed significant alterations under different glucose concentrations (5.5 mM, 15 mM, and 25 mM) (Supplementary Figure S3). These results indicate that a high glucose environment induces a high-glycolytic phenotype and a low glucose environment induces a low-glycolytic phenotype in GC cells. Thus, these culture conditions were used for subsequent cell models.

High-glucose environment promotes malignant phenotypes in GC cells. Changes in the functional phenotypes of GC cells in high- and low-glucose culture environments were determined. The proliferation rates of GC cells cultured in a high-glucose environment were significantly higher than the proliferation rates of cells cultured in a low-glucose environment (Figure 4A). Colony formation assays demonstrated that the number of colonies formed increased with higher glucose concentrations (Supplementary Figure S4A). Thus, increased glycolysis significantly enhances the proliferative capacity of GC cells. The numbers of migrating and invading cells were significantly higher in the high-glucose culture group compared with the numbers in the low-glucose culture group, indicating that the migration and invasion abilities of GC cells increased under high-glucose conditions (Figure 4B, Supplementary Figure S4B). Sphere formation assays indicated that the number of spheres formed by GC cells significantly increased in cells cultured in high-glucose concentrations compared with the number of spheres in cells cultured in low-glucose conditions, indicating that

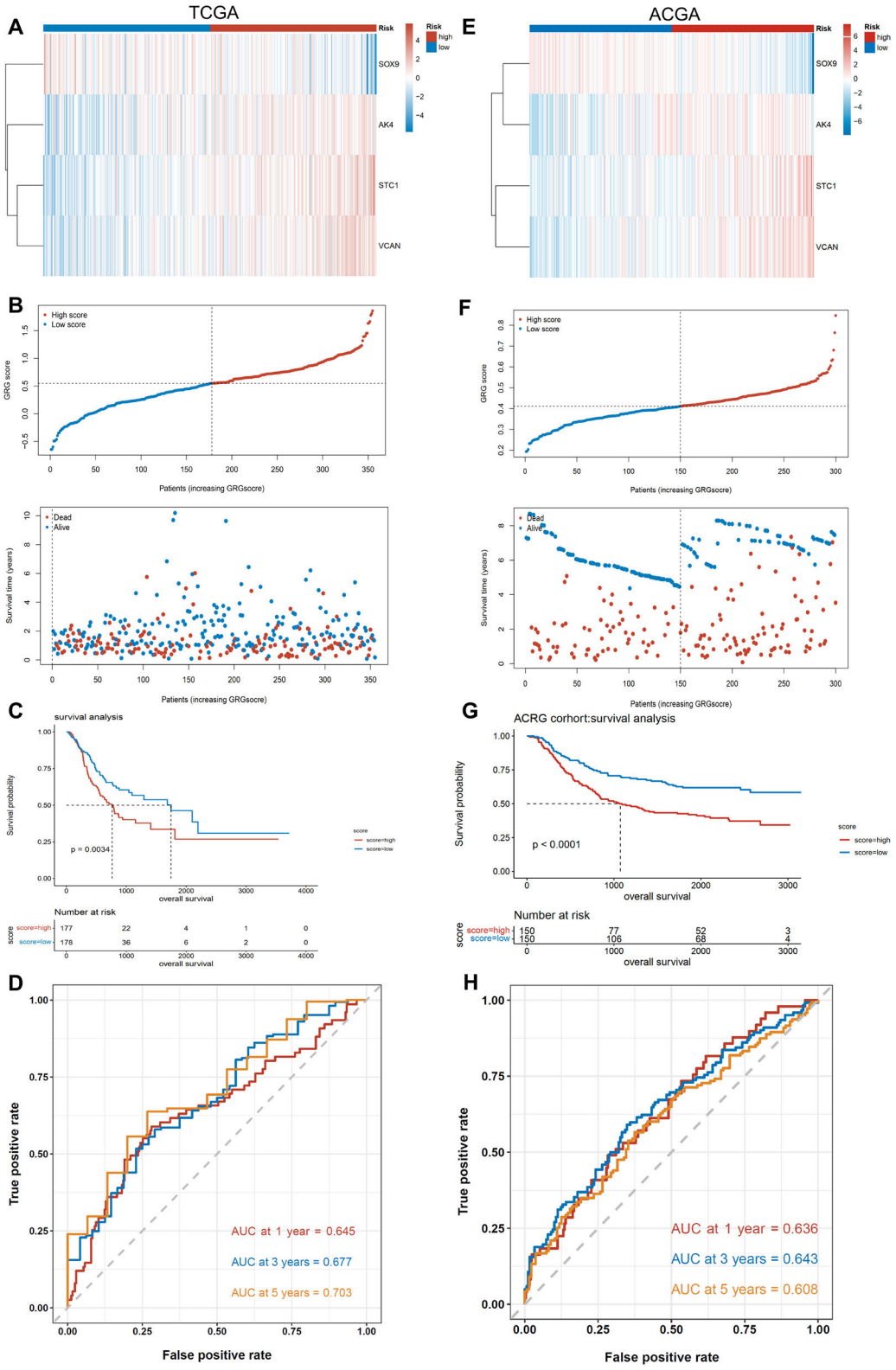

Figure 1. Glycolysis-related gene (GRG) score analyses in patients with gastric cancer (GC) in the training and testing sets based on the four GRGs. A) Heatmap of the four-GRG expression profile. B) Distribution of GRG scores per patient. C) Survival status and survival times of GC patients according to GRG scores. D) Kaplan-Meier plots showing overall survival (OS) in high- and low-GRG score groups. E, H) External validation of the GRG score using expression data from the ACGA database.

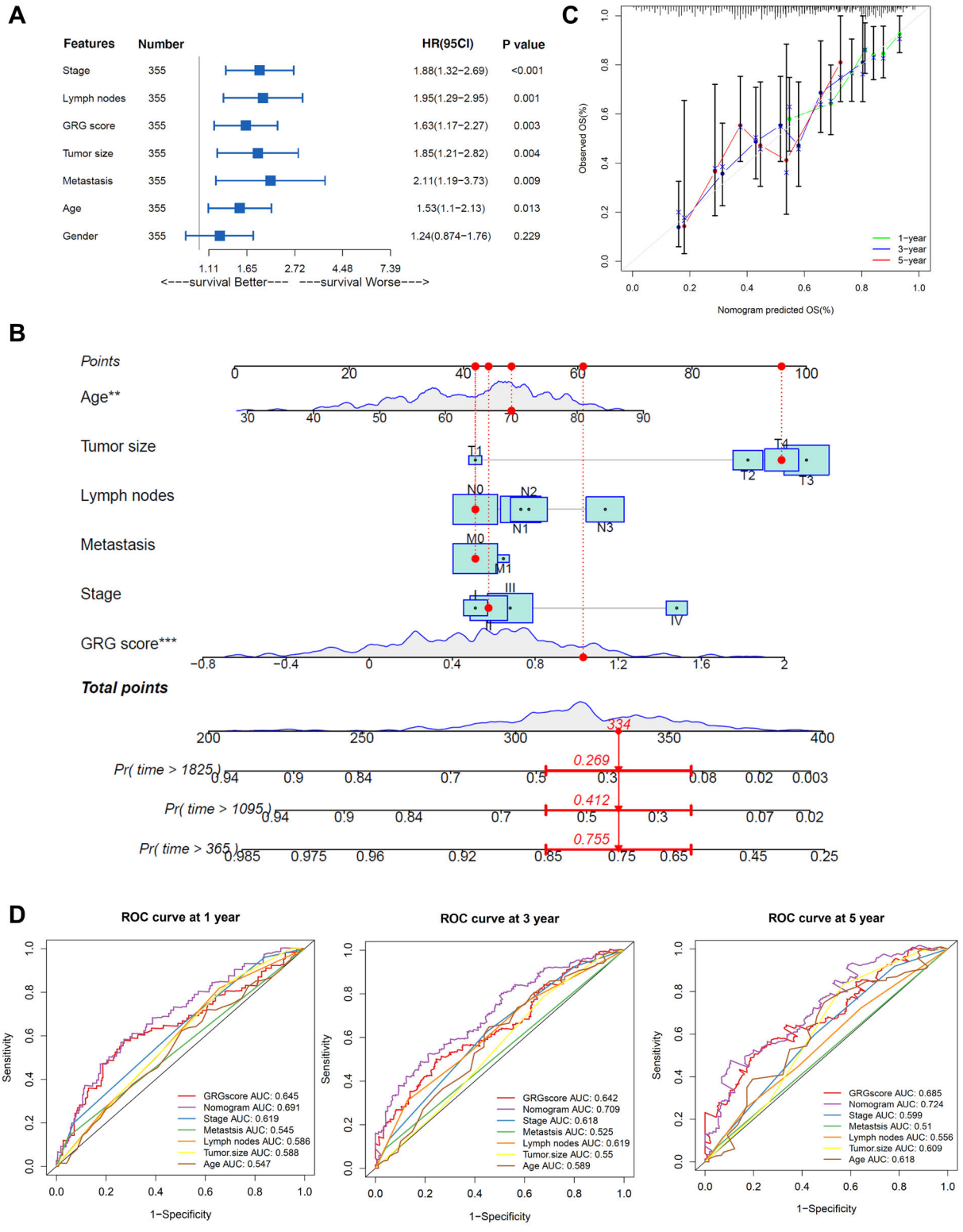

Figure 2. Combining glycolysis and clinical features to construct a nomogram for predicting the prognosis of GC patients. A) Forest plot illustrating the univariate Cox regression of the GRG scores and corresponding clinical features. B) Age, TNM, stage, and GRG score were employed in the Nomogram, and the total score was used to predict the 1-, 3-, and 5-year prognosis of patients with GC. C) Calibration curve of the Nomogram to predict survival within 5 years. D) Receiver operating characteristic (ROC) curves for predicting prognosis using different predictive models at 1 year, 3 years, and 5 years.

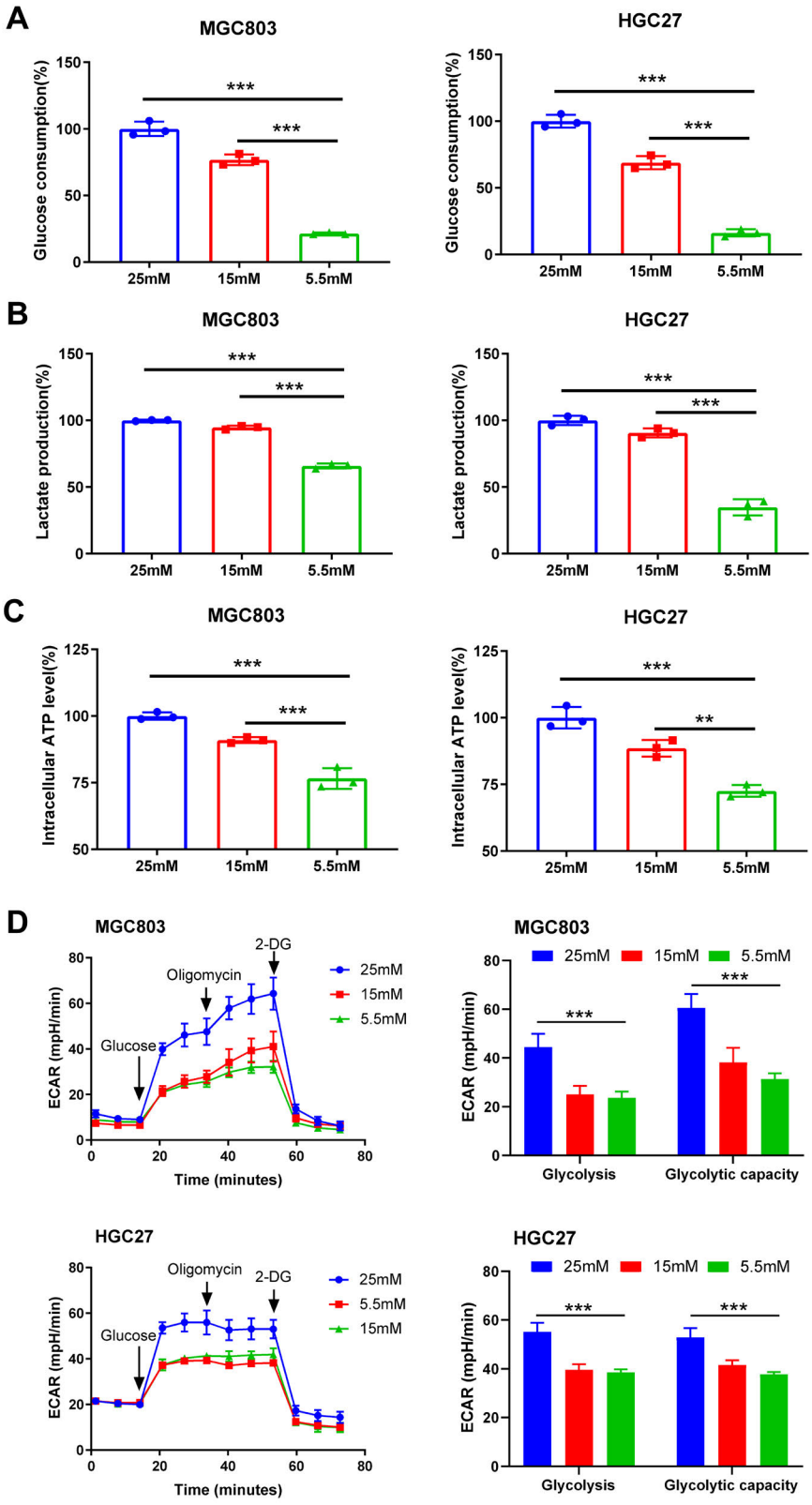

Figure 3. High and low glucose culture conditions induce high and low glycolytic phenotypes in GC cells. A) Glucose consumption, B) lactate production, C) intracellular adenosine 5'-triphosphate (ATP) production, and D) extracellular acidification rate (ECAR) in MGC803 and HGC27 cells cultured in different glucose concentrations. Data are shown as means ± SD. **p<0.01, ***p<0.001

the stem cell-like properties of GC cells were enhanced in a high-glucose environment (Figure 4C). Overall, these results demonstrate that increased glycolysis levels are associated with the malignant phenotype of GC cells, including metastasis and stemness, and a high-glucose environment promotes these malignant traits.

High-glucose environment promotes GC progression via the PI3K/AKT pathway. To further investigate the mechanisms by which high glucose regulates GC progression, DEGs in GC patients with high and low glycolysis in the TCGA-STAD dataset were analyzed. 2,248 genes were upregulated and 165 genes were downregulated in the high glycolysis group compared to the low glycolysis group (Figure 5A). DEGs were mainly enriched in biological functions such as extracellular matrix, cell adhesion, and migration, according to GO analysis (Supplementary Figure S5A). And KEGG analysis demonstrated that DEGs were mainly enriched in the PI3K/AKT pathway (Figure 5B). GSEA analysis further confirmed that PI3K/AKT (Figure 5C) was significantly enriched in GC with high glycolysis. This was further validated by western blot analysis (Figure 5D, Supplementary Figure S6A), which demonstrated increased activation of PI3K/AKT in GC cells with increasing glucose concentrations in the culture environment. Collectively, these results suggest that high glycolysis in GC enhances malignant phenotypes such as metastasis and stemness by activating the PI3K/AKT signal pathway.

High-glucose environment promotes EMT and stemness in GC. The GSEA analysis indicated that the EMT and P53 pathways were significantly enriched in the high glycolysis group within the hallmark gene sets (Supplementary Figure S5B). Based on previous findings on the functional phenotypes of GC cells, it is tenable to hypothesize that a high-glucose environment influences EMT and stemness in GC. The EMTome database [15] was utilized to download a pan-cancer 78-gene EMT signature, which was employed to construct an EMT score. EMT scores were significantly elevated in the high glycolysis group compared with the EMT scores in the low glycolysis group (Figure 6A), and EMT scores significantly correlated with GRG scores (Figure 6B). Expression levels of EMT-related markers (N-cadherin, vimentin, and snail) were significantly higher in GC cells cultured in a high-glucose environment compared with cells cultured in a low-glucose environment (Figure 6C, Supplementary Figure S6B), confirming that increased glycolysis promotes EMT in GC cells.

A stemness score was constructed using 109 tumor stem cell genes, as previously described [16]. Stemness scores were significantly elevated in the high glycolysis group compared to the scores in the low glycolysis group (Figure 6D); GRG scores significantly correlated with stemness (Figure 6E). Western blot analysis confirmed the stemness-related molecular phenotype in GC cells. The expression levels of stemness-related markers (CD44, OCT4, and SOX2) were significantly higher in GC cells cultured in a high-glucose environment compared with the expression levels in GC cells cultured in a low-glucose environment (Figure 6F, Supplementary Figure S6C). Thus, elevated glycolysis influences stemness in GC cells.

Discussion

Despite recent advances in the diagnosis and treatment of GC, drug resistance is associated with low survival rates. Thus, identifying novel therapeutic targets and strategies for patients with GC is urgently needed [17]. High blood glucose levels are associated with poorer prognoses in cancer patients, including those with GC [18, 19]. Diabetes is known to increase the risk of various cancers, such as liver, pancreatic, colorectal, and GCs. Most cancer patients with uncontrolled plasma glucose levels have poorer prognoses and shorter survival times [20, 21]. This highlights the impact of glucose metabolism on tumor stemness and metastasis [22, 23].

Increasing evidence suggests that relying on single clinical factors or individual gene characteristics often results in poor predictive performance. Now, we can focus on identifying a series of the most critical genes related to patient survival predictions, rather than conducting broad explorations. We constructed a high glycolysis score model (GRG score) based on clinical data and demonstrated that high glucose levels affect the prognosis of patients with GC, consistent with previous research findings [22, 23]. Subsequent survival analysis revealed that patients in the high GRG score group had worse prognoses. This result was validated with an independent ACGA cohort. The distribution of GRG scores differed significantly across molecular subtypes, with enrichment of high glycolysis in the GS subtype. These findings suggest that metabolic phenotypes may complement genomic classifications and offer an additional layer of tumor stratification, potentially paving the way for refined prognostic and therapeutic frameworks. GRG scores and clinical characteristics were combined into a nomogram. The nomogram is an effective tool for the clinical diagnosis and treatment of GC patients. These results indicate that GRG scores and the nomogram strongly predict the prognosis of patients with GC and can guide clinical treatment decisions [24].

Subsequently, a high-glucose state was simulated *in vitro* by culturing cells in a high-glucose medium, thereby mimicking hyperglycemia. Prolonged exposure to elevated glucose levels increased glycolysis and enhanced malignancy-related phenotypes associated with cancer stemness [18]. The proliferation, migration, invasion, and self-renewal abilities of GC cells were significantly enhanced when exposed to high glucose. Active glycolysis is a hallmark of malignancy, typically accompanied by elevated levels of glycolytic enzymes and corresponding metabolites. Nevertheless, the precise mechanisms by which glycolysis contributes to tumorigenesis are unclear [25]. Increasing evidence indicates that metabolism, particularly glycolysis, and cancer stemness are intricately intertwined processes within tumor

tissues [26]. Tumor cells exhibit active glycolytic activity and a strong dependence on glycolysis [27]. Abnormal increases in glycolytic intermediates or products are markers of enhanced cancer stemness and chemoresistance [13]. Additionally, CSCs exhibit significantly increased glucose uptake and lactate production and reduced mitochondrial respiration [28]. Leveraging these metabolic changes may provide effective targeted therapeutic strategies, reducing the risk of recurrence and metastasis [29].

Regarding the molecular mechanisms of glucose-driven oncogenesis, glucose is widely recognized to promote cancer progression through various metabolic pathways. Tumor

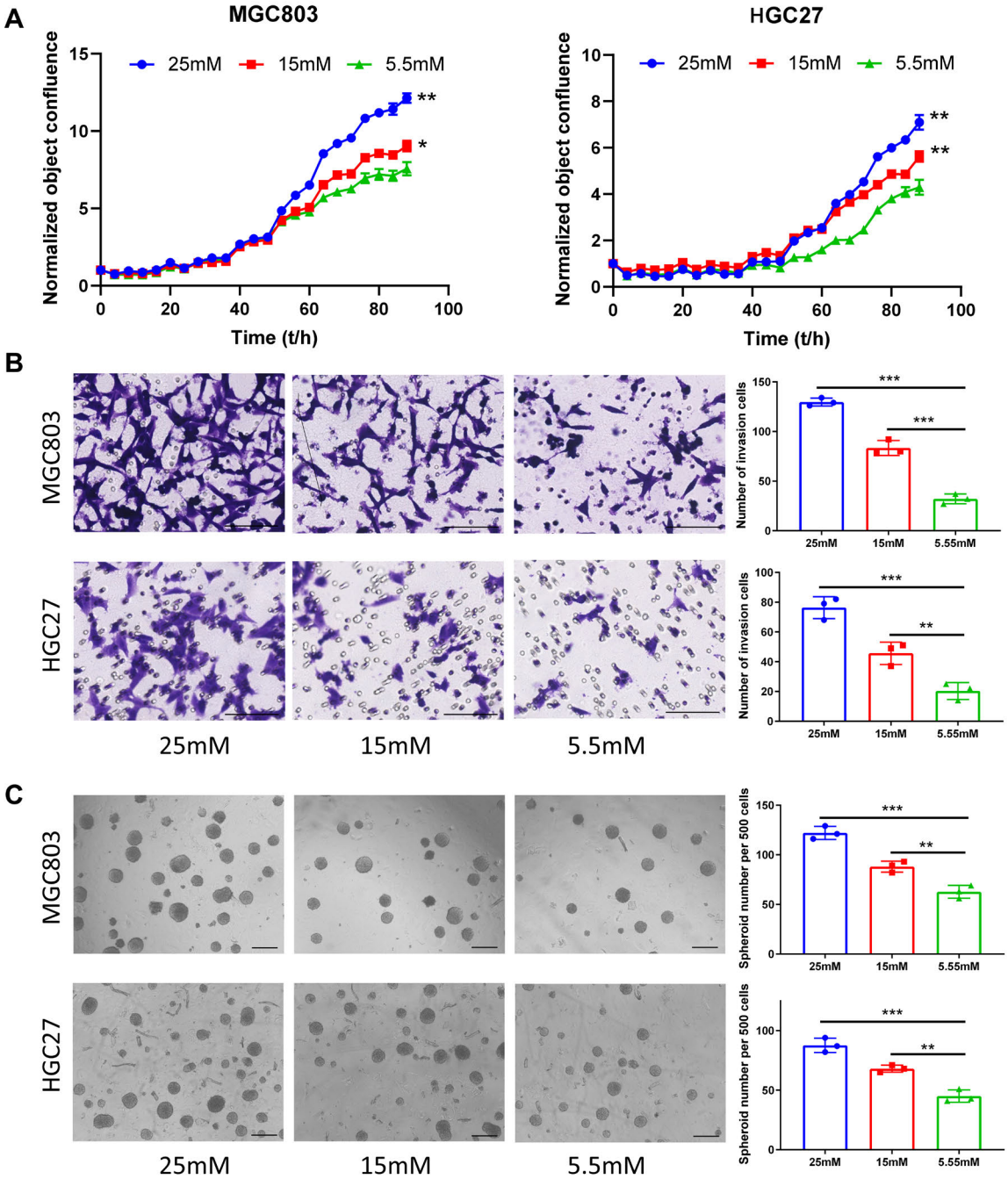

Figure 4. Culturing in different glucose concentrations affects the stem-related features of GC cells. A) Cell proliferation capacity, B) invasion ability (scale bar, 100 μm), and C) self-renewal ability (scale bar, 1000 μm) of MGC803 and HGC27 cells cultured in different glucose concentrations. Data are presented as means ± SD. *p<0.05, **p<0.01, ***p<0.001.

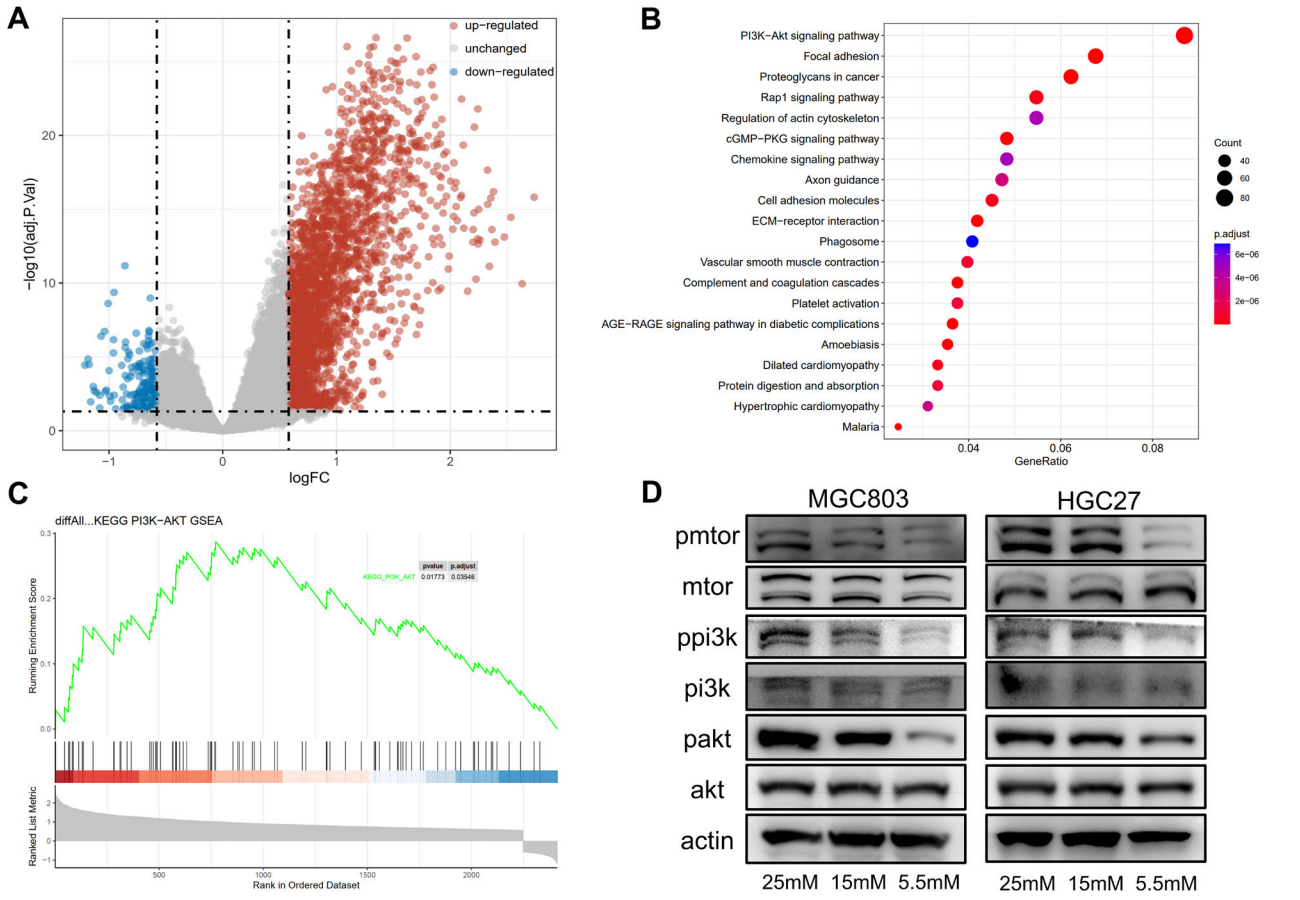

Figure 5. High-glucose environment culture contributes to the progression of GC via the PI3K/AKT pathway. A) Volcano plot showing the distribution of differentially expressed genes (DEGs) in high and low glycolysis-related gene (GRG) score groups. B) KEGG enrichment analysis of DEGs between the high and low GRG score groups. C) GSEA analysis of PI3K/AKT genes between the high and low GRG score groups. D) Western blots showing phosphorylation of proteins in the PI3K/AKT pathway in GC cells cultured in different glucose concentrations.

cells are capable of sensing extracellular glucose fluctuations and adaptively modulating intracellular metabolic flux, thereby regulating glycolytic activity and influencing stemness-related properties that contribute to tumor initiation and progression. In this study, we evaluated the effects of different glucose concentrations on glycolysis and oxidative phosphorylation (OXPHOS) by measuring ECAR and OCR, respectively. The results demonstrated that OXPHOS activity remained relatively stable across the tested glucose concentrations, whereas glycolytic activity, as indicated by ECAR, exhibited more pronounced dynamic changes in response to extracellular glucose levels.

Previous studies have shown that tumor cells display highly dynamic metabolic adaptations to glucose availability, with the magnitude and direction of these shifts largely dependent on tumor type and metabolic plasticity. For instance, in glioblastoma, lower glucose concentrations (100 mg/l) are associated with increased OCR, suggesting compensatory reliance on OXPHOS when glycolytic flux is restricted. In contrast, at higher glucose levels (1,000–4,500 mg/l), glycolytic reserve increases while OCR decreases, indicating a metabolic shift toward glycolysis [30]. Conversely, in breast cancer cells, glucose deprivation suppresses both ECAR and OCR, accompanied by ATP depletion, lactate reduction, mitochondrial depolarization, and activation of pyroptotic pathways [31]. These findings underscore the significant intertumoral variability in metabolic regulation and OXPHOS dependency.

Our findings further support the notion that GC cells exhibit a distinct form of metabolic flexibility, maintaining relatively stable mitochondrial respiration while dynamically adjusting glycolytic activity in response to extracellular glucose availability. These observations complement the broader understanding that glucose promotes cancer progression through multiple metabolic pathways, including glycolysis, the tricarboxylic acid cycle, glycosylation, and lipid synthesis. Such metabolic reprogramming contributes to the activation of oncogenic signaling pathways, enhancing tumor cell proliferation, metastasis, drug resistance, and angiogenesis. Furthermore, high glucose levels can upregu-

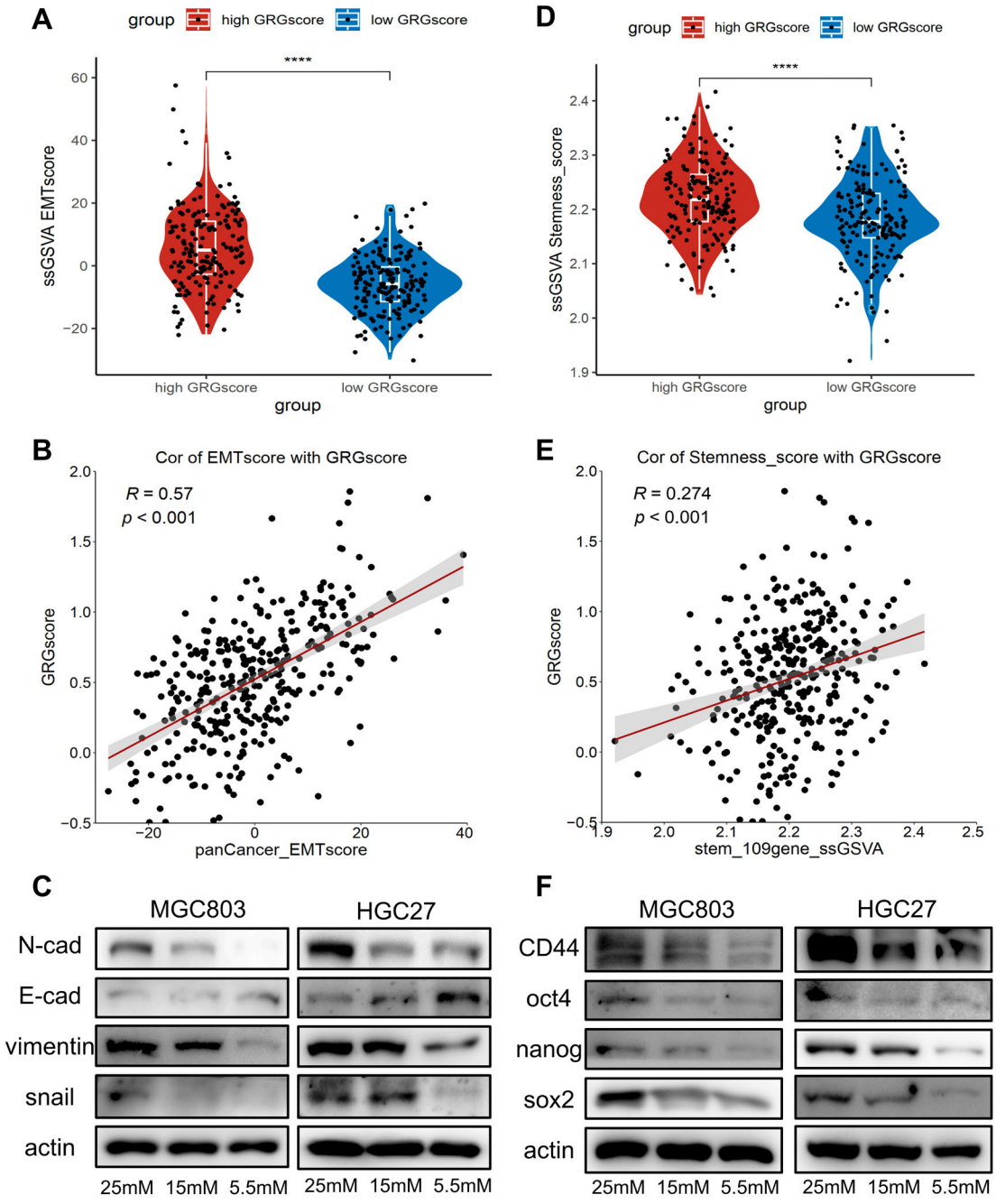

Figure 6. High-glucose environment promotes epithelial-mesenchymal transition (EMT) and stemness in GC. A) Violin plot comparing the distribution of the EMT scores in the high- and low-GRG score groups. B) Correlation between the EMT and GRG scores in TCGA database. C) Western blots showing expression of EMT-related markers in GC cells cultured in different glucose concentrations. D) Violin plot analysis comparing stemness scores in the high- and low-GRG score groups. E) Correlation between stemness and GRG scores in TCGA database. F) Western blots showing expression of stemness markers in GC cells cultured in different glucose concentrations.

late key enzymes in glucose metabolism, leading to increased glycolysis, glycosylation modifications, lactate production, and lipid synthesis. These alterations in energy metabolism activate signaling pathways associated with invasive tumor phenotypes [18, 32], promoting tumor cell proliferation, metastasis, drug resistance, and angiogenesis. Hyperglycemia, both directly and indirectly, is associated with an increased risk for carcinogenesis. The mechanisms through which hyperglycemia contributes to carcinogenic pathways are numerous and complex. These include direct or indirect

DNA damage, reactive oxygen species formation, mutation accumulation, impaired DNA repair, and aberrant regulation of oncogenes and tumor suppressor genes [33]. These metabolic reprogramming and tumor microenvironment modifications ultimately promote cancer development and progression. The p53 checkpoint bypasses independent of mutations may represent the carcinogenic origin and targetable susceptibility of glucose-driven cancers [34]. Additionally, glucose can promote cancer without being metabolized. Glucose functions as an oncogenic signaling molecule that directly binds to NSUN2, inhibiting the activation of the STING pathway. Suppression of the STING pathway impedes the activation and infiltration of antitumor T cells, ultimately promoting cancer initiation and progression [35].

Energy-responsive growth signaling pathways are implicated in metabolic reprogramming to support abnormal proliferation and metastasis [36, 37]. As a key oncogenic signaling pathway, PI3K/AKT has emerged as an important therapeutic target in cancer treatment due to its central role in regulating tumor cell proliferation, survival, metabolism, and resistance. Our results demonstrate the effects of high glucose-mediated glycolysis on the PI3K/AKT signaling in GC. This finding validates the impact of glycolysis on EMT and stemness-related biological and molecular phenotypes in tumor cells, consistent with previous studies [38]. Notably, several PI3K inhibitors have already been approved for clinical use in certain cancer types, and multiple PI3K/AKT-targeted agents are currently under active clinical investigation [39, 40]. Meanwhile, it is essential to acknowledge the constraints of our study when interpreting the results. The culturing of GC cells in varying glucose concentrations can only simulate a high-glucose environment and does not accurately represent the *in vivo* hyperglycemic environment. In addition, the current study is limited by the availability of cell models, and future investigations incorporating low-passage primary GC cells or patient-derived models would provide more clinically relevant insights. Furthermore, given that our analysis relies solely on retrospective TCGA data, future prospective clinical studies are needed to validate the relationship between blood glucose levels, therapeutic response, and tumor progression.

In conclusion, we demonstrate that elevated glycolysis is associated with worse clinical prognoses in patients with GC. A predictive model combining glycolysis and clinical features are developed and validated to assess patient prognosis. Additionally, we simulate a high-glucose environment by culturing GC cells in various glucose concentrations. This approach demonstrates that the high-glycolysis phenotype induced by a high-glucose environment significantly impacts malignant characteristics such as metastasis and stemness in GC cells. This mechanism may involve the PI3K/AKT pathway, which promotes EMT and regulates GC stemness by influencing glycolysis levels. Moving forward, we plan to investigate the mechanistic role of PI3K/AKT signaling through pharmacological inhibition and assess the therapeutic potential of combined targeting of glycolysis and the PI3K/AKT pathway. Our findings highlight the necessity for clinical attention to GC patients with hyperglycemia and present novel strategies and therapeutic targets for GC diagnosis and treatment by elucidating the underlying mechanisms.

Supplementary information is available in the online version of the paper.

Acknowledgments: This work was financially supported by National Key Research and Development Program of China (No.2022YFC2409902), National Natural Science Foundation of China (82073278), Beijing Municipal Health Commission (BMHC-2021-6, BJRITO-RDP-2023, XT-2024-06, JYY2023-11, JYY2023-8), CAMS Innovation Fund for Medical Sciences (2021-I2M-1-067), Middle-aged and Young Scientist Fund of Qinghai University Medical College (2023-kyt-2), Xining Science and Technology Bureau People's Livelihood Science and Technology Special Program (2019-M-15), The Independent Issue of State Key Laboratory of Molecular Oncology (SKLMO-2025-17).

References

[1] THRIFT AP, WENKER TN, EL-SERAG HB. Global burden of gastric cancer: epidemiological trends, risk factors, screening and prevention. Nat Rev Clin Oncol 2023; 20: 338–349. https://doi.org/10.1038/s41571-023-00747-0

[2] BRAY F, LAVERSANNE M, SUNG H, FERLAY J, SIEGEL RL et al. Global cancer statistics 2022: GLOBOCAN estimates of incidence and mortality worldwide for 36 cancers in 185 countries. CA Cancer J Clin 2024; 74: 229–263. https://doi.org/10.3322/caac.21834

[3] THRIFT AP, EL-SERAG HB. Burden of Gastric Cancer. Clin Gastroenterol Hepatol. 2020; 18: 534–542. https://doi.org/10.1016/j.cgh.2019.07.045

[4] TOKUNAGA M, SATO Y, NAKAGAWA M, ABURATANI T, MATSUYAMA T et al. Perioperative chemotherapy for locally advanced gastric cancer in Japan: current and future perspectives. Surg Today 2020; 50: 30–37. https://doi.org/10.1007/s00595-019-01896-5

[5] LOH JJ, MA S. Hallmarks of cancer stemness. Cell Stem Cell 2024; 31: 617–639. https://doi.org/10.1016/j.stem.2024.04.004

[6] CHEN H, ZHENG X, ZONG X, LI Z, LI N et al. Metabolic syndrome, metabolic comorbid conditions and risk of early-onset colorectal cancer. Gut 2021; 70: 1147–1154. https://doi.org/10.1136/gutjnl-2020-321661

[7] DONGRE A, WEINBERG RA. New insights into the mechanisms of epithelial-mesenchymal transition and implications for cancer. Nat Rev Mol Cell Biol 2019; 20: 69–84. https://doi.org/10.1038/s41580-018-0080-4

[8] MURPHY N, SONG M, PAPADIMITRIOU N, CARRERAS-TORRES R, LANGENBERG C et al. Associations Between Glycemic Traits and Colorectal Cancer: A Mendelian Randomization Analysis. J Natl Cancer Inst 2022; 114: 740–752. https://doi.org/10.1093/jnci/djac011

[9] HANAHAN D, WEINBERG RA. Hallmarks of cancer: the next generation. Cell 2011; 144: 646–674. https://doi.org/10.1016/j.cell.2011.02.013
[10] WARBURG O, WIND F, NEGELEIN E. The Metabolism of Tumors in the Body. J Gen Physiol 1927; 8: 519–530. https://doi.org/10.1085/jgp.8.6.519
[11] PAPADAKI S, MAGKLARA A. Regulation of Metabolic Plasticity in Cancer Stem Cells and Implications in Cancer Therapy. Cancers (Basel) 2022; 14. https://doi.org/10.3390/cancers14235912
[12] DI FRANCESCO AM, TOESCA A, CENCIARELLI C, GIORDANO A, GASBARRINI A et al. Metabolic Modification in Gastrointestinal Cancer Stem Cells: Characteristics and Therapeutic Approaches. J Cell Physiol 2016; 231: 2081–2087. https://doi.org/10.1002/jcp.25318
[13] CHEN K, ZHANG C, LING S, WEI R, WANG J et al. The metabolic flexibility of quiescent CSC: implications for chemotherapy resistance. Cell Death Dis 2021; 12: 835. https://doi.org/10.1038/s41419-021-04116-6
[14] YANG T, SHU X, ZHANG HW, SUN LX, YU L et al. Enolase 1 regulates stem cell-like properties in gastric cancer cells by stimulating glycolysis. Cell Death Dis 2020; 11: 870. https://doi.org/10.1038/s41419-020-03087-4
[15] MAK MP, TONG P, DIAO L, CARDNELL RJ, GIBBONS DL et al. A Patient-Derived, Pan-Cancer EMT Signature Identifies Global Molecular Alterations and Immune Target Enrichment Following Epithelial-to-Mesenchymal Transition. Clin Cancer Res 2016; 22: 609–620. https://doi.org/10.1158/1078-0432.CCR-15-0876
[16] MIRANDA A, HAMILTON PT, ZHANG AW, PATTNAIK S, BECHT E et al. Cancer stemness, intratumoral heterogeneity, and immune response across cancers. Proc Natl Acad Sci U S A 2019; 116: 9020–9029. https://doi.org/10.1073/pnas.1818210116
[17] MORGAN E, ARNOLD M, CAMARGO MC, GINI A, KUNZMANN AT et al. The current and future incidence and mortality of gastric cancer in 185 countries, 2020–40: A population-based modelling study. eClinicalMedicine 2022; 47. https://doi.org/10.1016/j.eclinm.2022.101404
[18] SUPABPHOL S, SEUBWAI W, WONGKHAM S, SAENGBOONMEE C. High glucose: an emerging association between diabetes mellitus and cancer progression. J Mol Med (Berl) 2021; 99: 1175–1193. https://doi.org/10.1007/s00109-021-02096-w
[19] HU Y, ZHANG X, MA Y, YUAN C, WANG M et al. Incident Type 2 Diabetes Duration and Cancer Risk: A Prospective Study in Two US Cohorts. J Natl Cancer Inst 2021; 113: 381–389. https://doi.org/10.1093/jnci/djaa141
[20] NIK-AHD F, HOWARD LE, EISENBERG AT, ARONSON WJ, TERRIS MK et al. Poorly controlled diabetes increases the risk of metastases and castration-resistant prostate cancer in men undergoing radical prostatectomy: Results from the SEARCH database. Cancer 2019; 125: 2861–2867. https://doi.org/10.1002/cncr.32141
[21] ZHENG J, XIE SH, SANTONI G, LAGERGREN J. Population-based cohort study of diabetes mellitus and mortality in gastric adenocarcinoma. Br J Surg 2018; 105: 1799–1806. https://doi.org/10.1002/bjs.10930
[22] HE X, CHENG X, DING J, XIONG M, CHEN B et al. Hyperglycemia induces miR-26-5p down-regulation to overexpress PFKFB3 and accelerate epithelial-mesenchymal transition in gastric cancer. Bioengineered 2022; 13: 2902–2917. https://doi.org/10.1080/21655979.2022.2026730
[23] XU X, CHEN B, ZHU S, ZHANG J, HE X et al. Hyperglycemia promotes Snail-induced epithelial-mesenchymal transition of gastric cancer via activating ENO1 expression. Cancer Cell Int 2019; 19: 344. https://doi.org/10.1186/s12935-019-1075-8
[24] SHEN G, LIU S, CAO Y, CHEN Z, WANG G et al. HSP90 co-regulates the formation and nuclear distribution of the glycolytic output complex to promote resistance and poor prognosis in gastric cancer patients. J Transl Med 2025; 23: 172. https://doi.org/10.1186/s12967-025-06196-w
[25] SANCHO P, BARNEDA D, HEESCHEN C. Hallmarks of cancer stem cell metabolism. Br J Cancer 2016; 114: 1305–1312. https://doi.org/10.1038/bjc.2016.152
[26] SHEN YA, CHEN CC, CHEN BJ, WU YT, JUAN JR et al. Potential Therapies Targeting Metabolic Pathways in Cancer Stem Cells. Cells 2021; 10. https://doi.org/10.3390/cells10071772
[27] PAUL S, GHOSH S, KUMAR S. Tumor glycolysis, an essential sweet tooth of tumor cells. Sem Cancer Biol 2022; 86: 1216–1230. https://doi.org/10.1016/j.semcancer.2022.09.007
[28] BRUNGS D, AGHMESHEH M, VINE KL, BECKER TM, CAROLAN MG et al. Gastric cancer stem cells: evidence, potential markers, and clinical implications. J Gastroenterol 2016; 51: 313–326. https://doi.org/10.1007/s00535-015-1125-5
[29] KROEMER G, POUYSSEGUR J. Tumor cell metabolism: cancer's Achilles' heel. Cancer Cell 2008; 13: 472–482. https://doi.org/10.1016/j.ccr.2008.05.005
[30] MIKI K, YAGI M, YOSHIMOTO K, KANG D, UCHIUMI T. Mitochondrial dysfunction and impaired growth of glioblastoma cell lines caused by antimicrobial agents inducing ferroptosis under glucose starvation. Oncogenesis 2022; 11: 59. https://doi.org/10.1038/s41389-022-00437-z
[31] YE J, HU P, ZHANG R, ZHOU L, LUO Z et al. Targeting Hyperglycemic Bone Pre-Metastatic Niche for Breast Cancer Bone Metastasis Therapy. Adv Sci (Weinh) 2025: e04924. https://doi.org/10.1002/advs.202504924
[32] LIU S, SHEN G, ZHOU X, SUN L, YU L et al. Hsp90 Promotes Gastric Cancer Cell Metastasis and Stemness by Regulating the Regional Distribution of Glycolysis-Related Metabolic Enzymes in the Cytoplasm. Adv Sci (Weinh) 2024: e2310109. https://doi.org/10.1002/advs.202310109
[33] RAMTEKE P, DEB A, SHEPAL V, BHAT MK. Hyperglycemia Associated Metabolic and Molecular Alterations in Cancer Risk, Progression, Treatment, and Mortality. Cancers (Basel) 2019; 11. https://doi.org/10.3390/cancers11091402
[34] SU Y, LUO Y, ZHANG P, LIN H, PU W et al. Glucose-induced CRL4(COP1)-p53 axis amplifies glycometabolism to drive tumorigenesis. Mol Cell 2023; 83: 2316–2331.e2317. https://doi.org/10.1016/j.molcel.2023.06.010
[35] CHEN T, XU ZG, LUO J, MANNE RK, WANG Z et al. NSUN2 is a glucose sensor suppressing cGAS/STING to maintain tumorigenesis and immunotherapy resistance. Cell Metab 2023; 35: 1782–1798.e1788. https://doi.org/10.1016/j.cmet.2023.07.009

[36] SUN Y, ZHANG X, HANG D, LAU HC, DU J et al. Integrative plasma and fecal metabolomics identify functional metabolites in adenoma-colorectal cancer progression and as early diagnostic biomarkers. Cancer Cell 2024; 42: 1386–1400.e1388. https://doi.org/10.1016/j.ccell.2024.07.005

[37] SEMENTINO E, HASSAN D, BELLACOSA A, TESTA JR. AKT and the Hallmarks of Cancer. Cancer Res 2024; 84: 4126–4139. https://doi.org/10.1158/0008-5472.Can-24-1846

[38] SHU X, CAO KY, LIU HQ, YU L, SUN LX et al. Alpha-enolase (ENO1), identified as an antigen to monoclonal antibody 12C7, promotes the self-renewal and malignant phenotype of lung cancer stem cells by AMPK/mTOR pathway. Stem Cell Res Ther 2021; 12: 119. https://doi.org/10.1186/s13287-021-02160-9

[39] FONTANA F, GIANNITTI G, MARCHESI S, LIMONTA P. The PI3K/Akt Pathway and Glucose Metabolism: A Dangerous Liaison in Cancer. Int J Biol Sci 2024; 20: 3113–3125. https://doi.org/10.7150/ijbs.89942

[40] OCCHIUZZI MA, LICO G, IOELE G, DE LUCA M, GAROFALO A et al. Recent advances in PI3K/PKB/mTOR inhibitors as new anticancer agents. Eur J Med Chem 2023; 246: 114971. https://doi.org/10.1016/j.ejmech.2022.114971

Neoplasma 2025; 72(4): 300–306

doi:10.4149/neo_2025_250212N74

Temozolomide and anlotinib as second-line therapy for non-small cell lung cancer patients with brain metastases: a retrospective cohort study

Kaiyan LIU[1], Binfeng LI[2], Zhengkai XIANG[2], Jing TANG[3], Xiaobing LI[4,*]

[1]Department of Urology, Zhejiang Provincial People's Hospital, Hangzhou, China; [2]Department of Thoracic Surgery, Hubei Cancer Hospital, Tongji Medical College, Huazhong University of Science and Technology, Wuhan, China; [3]Department of Lymphoma, Hubei Cancer Hospital, Tongji Medical College, Huazhong University of Science and Technology, Wuhan, China; [4]Department of Thoracic Oncology, Hubei Cancer Hospital, Tongji Medical College, Huazhong University of Science and Technology, Wuhan, China

**Correspondence: lixiaobing0629@126.com*

Received February 12, 2025 / Accepted July 10, 2025

Brain metastases (BM) are a common and challenging complication of advanced non-small cell lung cancer (NSCLC). This study aimed to evaluate the efficacy and safety of the combination of temozolomide (TMZ) and anlotinib as a second-line treatment in advanced NSCLC patients with BM. Clinical data of advanced NSCLC patients with BM between January 2020 and December 2023 were retrospectively reviewed and analyzed. All patients received TMZ combined with anlotinib as a second-line treatment. The primary endpoints included overall survival (OS), progression-free survival (PFS), objective response rate (ORR), disease control rate (DCR), and adverse events (AEs). A total of 52 patients were enrolled, with 20 females and 32 males. The median PFS and OS were 5.0 months and 10.0 months. The ORR and DCR were 25% and 65%, respectively. Subgroup analysis demonstrated that patients who developed AEs such as hypertension, proteinuria, and hand-foot syndrome, as well as those with a favorable diagnosis-specified graded prognosis assessment score, had better efficacy outcomes, indicating these features may help to identify the priority population for this regimen. Common AEs, including hematological toxicity, fatigue, and hypertension, were generally manageable with dose adjustments and supportive care. TMZ combined with anlotinib could be a safe and effective second-line treatment option for advanced NSCLC patients with BM. Prospective trials are warranted to confirm these findings and optimize the treatment strategy.

Key words: temozolomide; anlotinib; brain metastasis; NSCLC

Non-small cell lung cancer (NSCLC) is the most common type of lung cancer and the leading cause of cancer-related mortality worldwide [1]. Over recent decades, significant advances have been made in NSCLC; however, patients with distant metastasis, especially brain metastasis (BM), still face unsatisfactory outcomes. BM occur in 25–40% of advanced NSCLC patients and significantly worsen prognosis and quality of life, with median survival ranging from 4–6 months without treatment [2].

The management of BM involves a combination of modalities, including surgery, whole-brain radiation therapy (WBRT), stereotactic radiosurgery (SRS), and systemic therapy. However, the optimal treatment approach remains undefined, particularly for patients with progressive disease after first-line therapy [3].

Temozolomide (TMZ) is an oral alkylating agent with activity against BM in various solid tumors [4], including NSCLC, glioblastoma multiforme (GBM) [5], and melanoma [6]. However, its efficacy as monotherapy is limited, with response rates ranging from 5–10% [7].

Anlotinib is a novel multi-targeted tyrosine kinase inhibitor (TKI) that inhibits angiogenesis and tumor growth through blocking VEGFR, PDGFR, FGFR, and other kinases [8]. It has shown promising efficacy in the treatment of advanced NSCLC, both as a monotherapy and in combination therapies. Preclinical studies have suggested that anlotinib may penetrate the blood-brain barrier and exert anti-cancer function in the CNS [9].

Given the limited efficacy of single-agent TMZ and the promising feature of anlotinib, their combination may represent a rational regimen for treating advanced NSCLC with BM. This study evaluates the efficacy and safety of TMZ combined with anlotinib as a second-line therapy in this setting and explores potential predictors for treatment response.

Patients and methods

Study design. This retrospective study evaluated the efficacy and safety of TMZ combined with anlotinib as a second-line treatment in advanced NSCLC patients with BM. The patients received second-line treatment at Hubei Cancer Hospital between January 2020 to December 2023.

Ethics approval. The study complied with the principles outlined in the Declaration of Helsinki (revised in 2013). Ethical approval for this retrospective trial was obtained from the Ethics Committee of Hubei Cancer Hospital, affiliated with Tongji Medical College, Wuhan, China (Approval No. HBCHEC2020201). Informed consent was waived due to its retrospective nature.

Patient selection. Patients eligible for inclusion met the following criteria: 1) histologically documented diagnosis of NSCLC; 2) presence of BM; 3) progression after first-line treatment; 4) ECOG performance status of 0–2; 5) sufficient organ function; and 6) complete medical records. Exclusion criteria included active systemic disease, prior TMZ or anlotinib treatment, or concurrent malignancies.

Treatment protocol. TMZ was administered intravenously at a dose of 150 mg/m² every three weeks, combined with oral anlotinib at 12 mg/day for two weeks, followed by a one-week break (three-week cycle). Dose reductions of anlotinib to 10 mg or 8 mg were permitted in the event of severe AEs. Treatment continued until progression or intolerable toxicity.

Efficacy evaluation. The primary endpoints included overall survival (OS), progression-free survival (PFS), objective response rate (ORR), disease control rate (DCR), and adverse events (AEs). OS is defined as the time from the initiation of second-line therapy to death from any cause; PFS is defined as the time from the start of treatment to disease progression or death. For patients with no available data on death or disease progression, data were censored at the last known follow-up date. BM was assessed using enhanced magnetic resonance imaging (MRI) or computed tomography (CT) scans, performed prior to and during regular follow-up visits. Tumor responses were evaluated using the Response Evaluation Criteria in Solid Tumors (RECIST) 1.1 and the revised Response Assessment in Neuro-Oncology Brain Metastasis (RANO-BM) criteria.

Safety evaluation. AEs were graded based on the National Cancer Institute Common Terminology Criteria for Adverse Events (NCI-CTCAE) version 5.0. hematologic and non-hematologic toxicities, including fatigue, hypertension, proteinuria, and hand-foot syndrome, were recorded and managed accordingly.

Statistical analysis. Data analysis was performed using SPSS 13.0 software. Descriptive summaries of PFS and OS were provided, along with their two-sided 95% confidence intervals (CIs). PFS and OS were estimated using the Kaplan-Meier method, and corresponding graphs were generated using Graph Prism 5.0. A p-value of less than 0.05 was considered statistically significant.

Results

Patient characteristic. In total, 52 patients were enrolled. 20 were females and 32 were males, with an average age of 67 years. Most males were heavy smokers, while females were predominantly non-smokers. Lung adenocarcinoma was the most common histological subtype, followed by

Table 1. Baseline clinical characteristics of the study cohort.

Characteristics	No. of patients (%)
Age	
years	67
range	47–75
Gender	
male	32 (61.54%)
female	20 (38.46%)
Smoking history	
never smoker	15 (28.85%)
former smoker	37 (71.15%)
Histology	
adenocarcinoma	31 (59.62%)
squamous carcinoma	21 (40.38%)
ECOG score	
0–1	39 (75.00%)
≥2	13 (25.00%)
GPA score	
0–1	8 (15.38%)
1.5–2.0	13 (25.00%)
2.5–3.0	14 (26.92%)
3.5–4.0	17 (32.69%)
Number of metastatic lesions	
single lesion (1 lesion)	11 (21.15%)
oligometastatic disease (2–4 lesions)	15 (28.85%)
multiple metastases (5–10 lesions)	16 (30.77%)
disseminated metastases (> 10 lesions)	10 (19.23%)
PD–L1 expression level	
<1%	26 (50.00%)
1–49%	16 (30.77%)
>>50%	10 (19.23%)
Previous Radiotherapy	
yes	15 (28.85%)
no	37 (71.15%)
Brain metastasis	
measurable	13 (25.00%)
unmeasurable	39 (75.00%)
Bone metastasis	
yes	37 (71.15%)
no	15 (28.85%)
Liver metastasis	
yes	9 (17.31%)
no	43 (82.69%)
Stage	
IVA	8 (15.38%)
IVB	20 (38.46%)
IVC	24 (46.15%)

squamous cell lung carcinoma (SqcLC). Approximately 75% of the patients had measurable BM. The Eastern Cooperative Oncology Group (ECOG) performance status ranged from 0 to 2. Most patients were EGFR wild-type, with three harboring EGFR mutation post-TKI progression. In terms of the proportion of patients classified by the number of brain metastases at enrollment, the proportions of patients with single lesion (1 lesion), oligometastatic disease (2–4 lesions), multiple metastases (5–10 lesions), and disseminated metastases (>10 lesions) were 11 (21.15%), 15 (28.85%), 16 (30.77%), and 10 (19.23%), respectively. (Table 1).

Prior treatment. Most patients (EGFR wild type) had received two or more lines of chemotherapy, commonly pemetrexed plus platinum or docetaxel/gemcitabine plus platinum in the first-line therapy. 28.85% of patients underwent WBRT ≥3 months prior. EGFR-mutant patients had been treated with TKI (icotinib, erlotinib, or gefitinib). Additional testing confirmed mutations including T790M and L858R, guiding subsequent osimertinib or standard chemotherapy (Table 1).

Efficiency. As of the data cutoff date, all patients had received the combination therapy of TMZ and anlotinib for at least two cycles, with an average of three cycles. No complete responses were observed; 13 patients had a partial response, 21 patients achieved stable disease, and 18 patients progressed. DCR was 65.38% and ORR was 25.00%. Intracranial and extracranial ORR were 5% and 20%, respectively. Median PFS and OS were 5.0 months (95% CI 3.97–5.64) and 10.0 months (95% CI 7.56–10.90) (Table 2, Figures 1A, 1B). Aside from therapeutic efficacy, in terms of quality-of-life improvement, the proportion of patients whose performance status (ECOG score) improved from 1 to 0 reached 50%, and the proportion of those whose score improved from 2 to 1 was nearly 15%. As most patients experienced significant improvements in quality of life after treatment, the proportion of those requiring long-term bed rest significantly decreased. Due to side effects, only less than 10% of patients required long-term bed rest because of treatment-related toxicity.

Biomarker exploration. Subgroup analyses revealed that PD-L1 status was not associated with a difference in efficacy. Patients with PD-L1 positive (+) (≥1%) and PD-L1 negative (–) (<1%) demonstrated the same mPFS and mOS (PD-L1 positive (+) vs. PD-L1 negative (–): mPFS 5.0 months vs. 5.0 months, p=0.58, HR=1.00, 95% CI 0.42–1.58; mOS 10.0 months vs. 10.0 months, p=0.78, HR=1.00, 95% CI 0.42–1.58, (Figures 1C, 1D). However, patients who experienced AEs, such as hypertension, proteinuria, or hand-foot syndrome, generally had better treatment outcomes compared to those who did not (with sAE vs. without sAE: mPFS 6.0 months vs. 4.0 months, p<0.0001, HR=1.50, 95% CI 0.94–2.07; mOS 10.5 months vs. 9.0 months, p<0.0001, HR=1.17, 95% CI 0.60–1.73; Figures 1E, 1F). Ds-GPA score correlated with the outcome that lower ds-GPA scores predict longer PFS and OS (GPA score (0–1) vs. (1.5–2) vs. (2.5–3) vs. (3.5–4), mPFS: 6.0 months vs. 5.0 months vs. 5.0 months vs. 4.0 months, p<0.0001; mOS 10.5 months vs. 10.0 months vs. 9.0 months vs. 8.0 months, p<0.0001, Figures 1G, 1H).

Table 2. Clinical activity of anlotinib plus TMZ in advanced NSCLC with BM.

	Patient No.	Ratio
Complete response	0	0
Partial response	13	25.00% (13/52)
Stable response	21	40.38% (21/52)
Progressive disease	18	34.62% (18/52)
Objective response		25.00%
Median PFS		5.0 months
Disease control rate		65.38%
Median OS		10.0 months

Table 3. Adverse events of anlotinib plus TMZ in advanced NSCLC with BM.

	anlotinib plus TMZ [n (%)]	
Adverse Event	**Any Grade**	**Grade 3 or 4**
Hematological		
Leukopenia	18 (34.62%)	3 (5.77%)
Neutropenia	17 (32.69%)	3 (5.77%)
Anemia	10 (19.23%)	0%
Thrombocytopenia	15 (28.85%)	2 (3.85%)
Nonhematologic		
Hypertension	14 (26.92%)	3 (5.77%)
Hand-foot syndrome	16 (30.77%)	3 (5.77%)
Proteinuria	10 (19.23%)	3 (5.77%)
Elevated transaminase	8 (15.38%)	3 (5.77%)
Hyperbilirubinemia	3 (5.77%)	0%
Bleeding	0%	0%
Fatigue	18 (34.62%)	0%
ALP increased	3 (5.77%)	0%
Elevated GGT	4 (7.69%)	0%
Abdominal pain	5 (9.62%)	0%
Decreased appetite	25 (48.08%)	0%
Hypoproteinemia	4 (7.69%)	0%
Diarrhea	6 (11.54%)	0%
Elevated LDH	3 (5.77%)	0%
Oral ulcer	6 (11.54%)	0%
Stomatitis	7 (13.46%)	0%
Dysphagia	5 (9.62%)	0%
Dysphonia	4 (7.69%)	0%
Rash	3 (1.92%)	0%

Toxicity. Common AEs included neutropenia, leukopenia, thrombocytopenia, anemia, decreased appetite, fatigue, hand-foot syndrome, hypertension, and proteinuria. Most were grade 1 or 2 and well tolerated. Grade 3 or 4 occurred in less than 40% of patients, including leukopenia, thrombocytopenia, neutropenia, hand-foot syndrome, hypertension, and proteinuria. Most of the AEs can be alleviated with supportive care. Treatment discontinuation occurred in 12%. (Table 3).

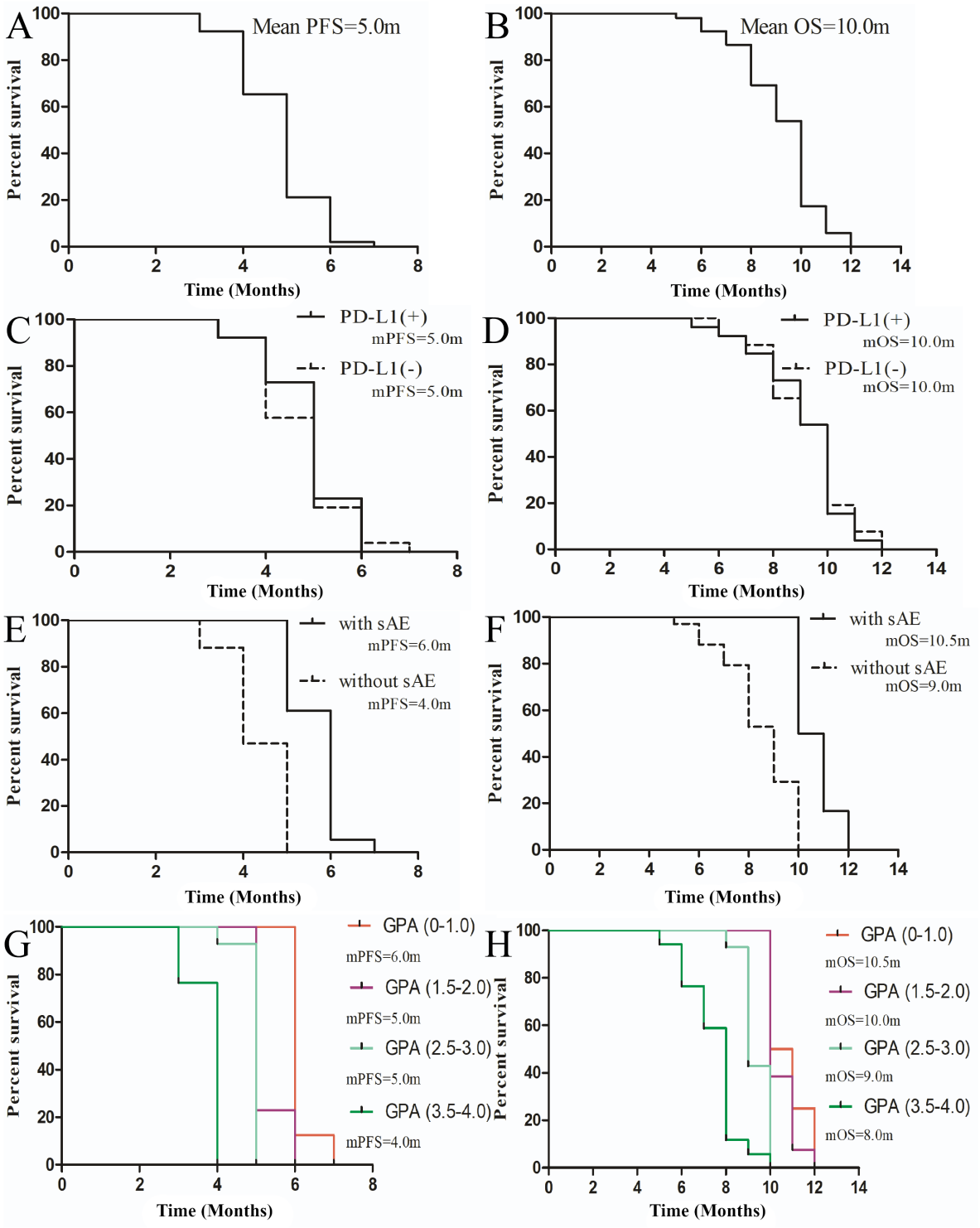

Figure 1. PFS and OS analysis of the general population and subgroup patients of advanced NSCLC with BM who accepted the drug combination of anlotinib and TMZ in this study. A, B) The overall PFS and OS in this study. C, D) Comparisons of PFS and OS between patients with different PD-L1 expression levels (PD-L1(+) vs. PD-L1(–)). E, F) Comparisons of PFS and OS between these patients with sAE and without sAE. G, H) Comparisons of PFS and OS among these patients according to the category of different dsGPA score. Abbreviations: mPFS-median progression-free survival; mOS-median overall survival; PD-L1-programmed death ligand 1; NSCLC-non-small cell lung cancer; Ds-GPA-Diagnosis-specified Graded Prognosis Assessment; Notes: PD-L1(+)-means PD-L1 ≥ 1%, while PD-L1(–) means PD-L1 (< 1%). sAE means specific Adverse Event (such as proteinuria, hypertension, or hand-foot syndrome)ç

Discussion

The treatment of advanced NSCLC with BM remains a major clinical challenge. Radiotherapy is the mainstay for BM, but it only provides short-term efficacy and is usually accompanied by comorbidities such as cognitive dysfunction [3]. Targeted therapies [10] and immune checkpoint inhibitors (ICIs) have been rapidly developed as cancer treatment modalities [10, 11]; nevertheless, their efficacy was limited in the setting of BM [12]. These limitations underscore the urgent need for further research and development in this field. Given the growing trend toward combination therapy, optimizing existing drug regimens may represent a promising strategy to improve outcomes for patients with BM [13–15].

In our study, we evidenced that the combination of TMZ and anlotinib demonstrated promising efficacy and manageable toxicity as a second-line treatment option for advanced NSCLC patients with BM.

The ORR of 25% observed in our cohort was extremely higher than that reported for monotherapy of TMZ (ORR less than 10%), or anlotinib alone (ORR of 14%), or ICIs (ORR of 9%). Furthermore, the median PFS and OS in our patients were 5.0 months and 10.0 months, which were dramatically longer than those reported for anlotinib monotherapy (PFS=4.0 months, OS=8.5 months) or ICIs (PFS=2.8 months, OS=7.5 months) [7, 9, 16]. Compared to previously reported clinical outcomes for combinations of anlotinib or TMZ with traditional treatment modalities such as radiotherapy, our results also revealed significant advantages in efficacy and safety [16–18].

Subgroup analyses revealed several clinical factors associated with treatment outcomes. Notably, patients experiencing sAE such as hypertension, proteinuria, or hand-foot syndrome demonstrated longer OS and PFS compared to those who did not [19]. This finding suggested that specific AEs may serve as potential prognostic markers. Additionally, the ds-GPA score also emerged as a significant prognostic indicator. Patients with lower ds-GPA scores presented superior OS and PFS [20]. This highlights the importance of personalized treatment strategies tailored to individual ds-GPA scores. Interestingly, contrary to previous studies indicating that PD-L1expression is positively associated with better response to immunotherapy and chemotherapy [21, 22], our findings showed no significant correlation between PD-L1 status and treatment efficacy. This discrepancy may reflect the distinct immune microenvironment features of BM [23]. Therefore, future strategies should prioritize individualized treatment planning based on stratification tools like ds-GPA. Further exploration of biomarkers and advanced imaging techniques may refine patient stratification and optimize treatment strategy [24, 25].

In terms of toxicity, the combination therapy was generally well-tolerated. The most common AEs were grade 1–2, including fatigue, hypertension, proteinuria, and hand-foot syndrome. Grade 3–4 hematological and non-hematological toxicities were infrequent and successfully managed with timely monitoring and supportive care [26–28].

As regards the potential mechanism of this combination, TMZ is known to enhance blood-brain barrier penetration, enabling anlotinib to enter the BM and exert antiangiogenic effect, thereby inhibiting tumor growth, proliferation, and metastasis [12, 29–31]. Therefore, TMZ mainly acts as a "gate opener" rather than a direct cytotoxic agent, allowing for reduced dosing without compromising the synergistic efficacy of the combination [29–35]. This regimen may improve patient tolerance and consequently enhance the quality of life.

In conclusion, the combination of TMZ and anlotinib appears to be an effective and tolerable regimen as a second-line treatment for advanced NSCLC patients with BM. Despite promising results, limitations such as retrospective nature, small sample size, and single-center design may restrict the generalizability of these findings. Future studies should focus on conducting larger-scale prospective trials to further establish the role of this combination in clinical practice [21–23].

Acknowledgments: The study was supported by the Natural Science Foundation of Hubei Province (No. 2019CFC929). We would like to thank Xichen Wang (MSD China, Shanghai, China) for providing academic information consulting support.

References

[1] OLIVER AL. Lung Cancer: Epidemiology and Screening. Surg Clin North Am 2022; 102: 335–344. https://doi.org/10.1016/j.suc.2021.12.001

[2] GILLESPIE CS, MUSTAFA MA, RICHARDSON GE, ALAM AM, LEE KS et al. Genomic Alterations and the Incidence of Brain Metastases in Advanced and Metastatic NSCLC: A Systematic Review and Meta-Analysis. J Thorac Oncol 2023; 18: 1703–1713. https://doi.org/10.1016/j.jtho.2023.06.017

[3] SUH JH, KOTECHA R, CHAO ST, AHLUWALIA MS, SAHGAL A et al. Current approaches to the management of brain metastases. Nat Rev Clin Oncol 2020; 17: 279–299. https://doi.org/10.1038/s41571-019-0320-3

[4] TATAR Z, THIVAT E, PLANCHAT E, GIMBERGUES P, GADEA E et al. Temozolomide and unusual indications: review of literature. Cancer Treat Rev 2013; 39: 125–135. https://doi.org/10.1016/j.ctrv.2012.06.002

[5] SUN M, HUANG N, TAO Y, WEN R, ZHAO G et al. The efficacy of temozolomide combined with levetiracetam for glioblastoma (GBM) after surgery: a study protocol for a double-blinded and randomized controlled trial. Trials 2022; 23: 234. https://doi.org/10.1186/s13063-022-06168-1

[6] HAN J, QIU M, SU L, WU C, CHENG S et al. Response and safety of whole-brain radiotherapy plus temozolomide for patients with brain metastases of non-small-cell lung cancer: A meta-analysis. Thorac Cancer 2021; 12: 3177–3183. https://doi.org/10.1111/1759-7714.14183

[7] GIORGIO CG, GIUFFRIDA D, PAPPALARDO A, RUSSO A, SANTINI D et al. Oral temozolomide in heavily pretreated brain metastases from non-small cell lung cancer: phase II study. Lung Cancer 2005; 50: 247–254. https://doi.org/10.1016/j.lungcan.2005.05.026

[8] HAN B, LI K, WANG Q, ZHANG L, SHI J et al. Effect of Anlotinib as a Third-Line or Further Treatment on Overall Survival of Patients With Advanced Non-Small Cell Lung Cancer: The ALTER 0303 Phase 3 Randomized Clinical Trial. JAMA Oncol 2018; 4: 1569–1575. https://doi.org/10.1001/jamaoncol.2018.3039

[9] JIANG S, LIANG H, LIU Z, ZHAO S, LIU J et al. The Impact of Anlotinib on Brain Metastases of Non-Small Cell Lung Cancer: Post Hoc Analysis of a Phase III Randomized Control Trial (ALTER0303). Oncologist 2020; 25: e870–e874. https://doi.org/10.1634/theoncologist.2019-0838

[10] WANG M, HERBST RS, BOSHOFF C. Toward personalized treatment approaches for non-small-cell lung cancer. Nat Med 2021; 27: 1345–1356. https://doi.org/10.1038/s41591-021-01450-2

[11] PAZ-ARES L, CIULEANU TE, COBO M, SCHENKER M, ZURAWSKI B et al. First-line nivolumab plus ipilimumab combined with two cycles of chemotherapy in patients with non-small-cell lung cancer (CheckMate 9LA): an international, randomised, open-label, phase 3 trial. Lancet Oncol 2021; 22: 198–211. https://doi.org/10.1016/S1470-2045(20)30641-0

[12] UPRETY D, REMON J, PETERS S. First-Line Dual Immunotherapy, a Treatment Option in First-Line Metastatic Non-Small-Cell Lung Cancer: Are We Ready to Use It? J Clin Oncol 2024; 42: 378–382. https://doi.org/10.1200/JCO.23.01524

[13] NADAL E, RODRÍGUEZ-ABREU D, SIMÓ M, MASSUTÍ B, JUAN O et al. Phase II Trial of Atezolizumab Combined With Carboplatin and Pemetrexed for Patients With Advanced Nonsquamous Non-Small-Cell Lung Cancer With Untreated Brain Metastases (Atezo-Brain, GECP17/05). J Clin Oncol 2023; 41: 4478–4485. https://doi.org/10.1200/JCO.22.02561

[14] PARK S, KIM TM, HAN JY, LEE GW, SHIM BY et al. Phase III, Randomized Study of Atezolizumab Plus Bevacizumab and Chemotherapy in Patients With EGFR- or ALK-Mutated Non-Small-Cell Lung Cancer (ATTLAS, KCSG-LU19-04). J Clin Oncol 2024; 42: 1241–1251. https://doi.org/10.1200/JCO.24.01092

[15] CABEBE E, WAKELEE H. Role of anti-angiogenesis agents in treating NSCLC: focus on bevacizumab and VEGFR tyrosine kinase inhibitors. Curr Treat Options Oncol 2007; 8: 15–27. https://doi.org/10.1007/s11864-007-0022-4

[16] ATTARIAN F, TAGHIZADEH-HESARY F, FANIPAKDEL A, JAVADINIA SA, POROUHAN P et al. A Systematic Review and Meta-Analysis on the Number of Adjuvant Temozolomide Cycles in Newly Diagnosed Glioblastoma. Front Oncol 2021; 11: 779491. https://doi.org/10.3389/fonc.2021.779491

[17] ANVARI K, SHAHABADI M, WELSH JS, JAVADINIA SA, ZAREI E. Outcome of Second Line Treatment of Recurrent High- Grade Glioma by re-Irradiation or Bevacizumab-based Chemotherapy: A Cross Sectional Study. Asian Pac J Cancer Prev 2023; 24: 1507–1511. https://doi.org/10.31557/APJCP.2023.24.5.1507

[18] ANVARI K, SEILANIAN TOUSSI M, SAGHAFI M, JAVADINIA SA, SAGHAFI H et al. Extended dosing (12 cycles) vs conventional dosing (6 cycles) of adjuvant temozolomide in adults with newly diagnosed high-grade gliomas: a randomized, single-blind, two-arm, parallel-group controlled trial. Front Oncol 2024; 14: 1357789. https://doi.org/10.3389/fonc.2024.1357789

[19] ZHANG C, KONG FW, WU WB, ZHANG M, YU GM et al. First-line pemetrexed and carboplatin plus anlotinib for epidermal growth factor receptor wild-type and anaplastic lymphoma kinase-negative lung adenocarcinoma with brain metastasis: A case report and review of the literature. Medicine (Baltimore) 2020; 99: e22128. https://doi.org/10.1097/MD.0000000000022128

[20] SPERDUTO PW, CHAO ST, SNEED PK, LUO X, SUH J et al. Diagnosis-specific prognostic factors, indexes, and treatment outcomes for patients with newly diagnosed brain metastases: a multi-institutional analysis of 4,259 patients. Int J Radiat Oncol Biol Phys 2010; 77: 655–661. https://doi.org/10.1016/j.ijrobp.2009.08.025

[21] Qiang H, Chang Q, Xu J, Qian J, Zhang Y et al. New advances in antiangiogenic combination therapeutic strategies for advanced non-small cell lung cancer. J Cancer Res Clin Oncol 2020; 146: 631–645. https://doi.org/10.1007/s00432-020-03129-6

[22] TSAKONAS G, DE PETRIS L, EKMAN S. Management of brain metastasized non-small cell lung cancer (NSCLC) - From local treatment to new systemic therapies. Cancer Treat Rev 2017; 54: 122–131. https://doi.org/10.1016/j.ctrv.2017.02.004

[23] OZCAN G, SINGH M, VREDENBURGH JJ. Leptomeningeal Metastasis from Non-Small Cell Lung Cancer and Current Landscape of Treatments. Clin Cancer Res 2023; 29: 11–29. https://doi.org/10.1158/1078-0432.CCR-22-1585

[24] XU Q, HUANG K, MENG X, WENG Y, ZHANG L et al. Safety and Efficacy of Anlotinib Hydrochloride Plus Temozolomide in Patients with Recurrent Glioblastoma. Clin Cancer Res 2023; 29: 3859–3866. https://doi.org/10.1158/1078-0432.CCR-23-0388

[25] LAI S, LI P, LIU X, LIU G, XIE T et al. Efficacy and safety of anlotinib combined with the STUPP regimen in patients with newly diagnosed glioblastoma: a multicenter, single-arm, phase II trial. Cancer Biol Med 2024; 21: 433–444. https://doi.org/10.20892/j.issn.2095-3941.2023.0373

[26] SI X, ZHANG L, WANG H, ZHANG X, WANG M et al. Management of anlotinib-related adverse events in patients with advanced non-small cell lung cancer: Experiences in ALTER-0303. Thorac Cancer 2019; 10: 551–556. https://doi.org/10.1111/1759-7714.12977

[27] Tang J, Jiang H, Xiang Z, Zhu X, Xie R et al. Apatinib plus docetaxel or pemetrexed shows promising activities against non-small cell lung cancer with brain metastasis: a retrospective analysis. J Thorac Dis 2024; 16: 615–622. https://doi.org/10.21037/jtd-23-1860

[28] LI X, WU D, TANG J, WU Y. The efficiency and safety of temozolomide and PD-1/L1 inhibitors in pretreated NSCLC with brain metastasis: a retrospective cohort. J Cancer Res Clin Oncol 2024; 150: 271. https://doi.org/10.1007/s00432-024-05808-0

[29] LAQUENTE B, VIÑALS F, GERMÀ JR. Metronomic chemotherapy: an antiangiogenic scheduling. Clin Transl Oncol 2007; 9: 93–98. https://doi.org/10.1007/s12094-007-0018-3

[30] YUAN F, SHI H, JI J, CAI Q, CHEN X et al. Capecitabine metronomic chemotherapy inhibits the proliferation of gastric cancer cells through anti-angiogenesis. Oncol Rep 2015; 33: 1753–1762. https://doi.org/10.3892/or.2015.3765

[31] KOLTAI T, CARDONE RA, RESHKIN SJ. Synergy Between Low Dose Metronomic Chemotherapy and the pH-centered Approach Against Cancer. Int J Mol Sci 2019; 20: 5438. https://doi.org/10.3390/ijms20215438

[32] BLUMBERG N. Tumor angiogenesis factor. Speculations on an approach to cancer chemotherapy. Yale J Biol Med 1974; 47: 71–81.

[33] SCHETTINO C, BARESCHINO MA, ROSSI A, MAIONE P, SACCO PC et al. Targeting angiogenesis for treatment of NSCLC brain metastases. Curr Cancer Drug Targets 2012; 12: 289–299. https://doi.org/10.2174/156800912799277476

[34] ILHAN-MUTLU A, SIEHS C, BERGHOFF AS, RICKEN G, WIDHALM G et al. Expression profiling of angiogenesis-related genes in brain metastases of lung cancer and melanoma. Tumour Biol 2016; 37: 1173–1182. https://doi.org/10.1007/s13277-015-3790-7

[35] ELLIS PM. Anti-angiogenesis in Personalized Therapy of Lung Cancer. Adv Exp Med Biol 2016; 893: 91–126. https://doi.org/10.1007/978-3-319-24223-1_5

https://doi.org/10.4149/neo_2025_250321N133

High glycolysis phenotype influences malignant progression and poor prognosis of gastric cancer through the PI3K/AKT pathway

Shiya LIU[1,#], Gaigai SHEN[1,#], Xuanyu ZHOU[2], Guanghui WANG[3], Huiqi LIU[3], Yuanting CAO[1], Lixin SUN[1,*], Xiong SHU[4,*], Yuliang RAN[1,*]

Supplementary Information

Supplementary Table S1. Clinic pathological characteristics of patients with gastric cancer with high and low GRG score in TCGA.

Characteristics	ALL N=355	high GRG score N=177	low GRG score N=178	OR	p-value
Age					
>65	187 (53.1%)	92 (52.0%)	95 (54.3%)		0.744
≤65	165 (46.9%)	85 (48.0%)	80 (45.7%)	0.912 [0.599;1.387]	
Gender					
female	125 (35.2%)	65 (36.7%)	60 (33.7%)		0.629
male	230 (64.8%)	112 (63.3%)	118 (66.3%)	1.141 [0.737;1.768]	
Metastasis					
M0	321 (93.3%)	159 (93.0%)	162 (93.6%)		0.977
M1	23 (6.69%)	12 (7.02%)	11 (6.36%)	0.901 [0.377;2.133]	
Lymph nodes					
N0	106 (30.8%)	47 (27.6%)	59 (33.9%)		
N1	93 (27.0%)	46 (27.1%)	47 (27.0%)	0.815 [0.464;1.428]	0.341
N2	69 (20.1%)	33 (19.4%)	36 (20.7%)	0.870 [0.471;1.604]	
N3	76 (22.1%	44 (25.9%)	32 (18.4%)	0.582 [0.318;1.054]	
Stage					
I	46 (13.5%)	15 (8.82%)	31 (18.1%)		
II	111 (32.6%)	58 (34.1%)	53 (31.0%)	0.446 [0.212;0.909]	0.094
III	151 (44.3%)	79 (46.5%)	72 (42.1%)	0.445 [0.216;0.882]	
IV	33 (9.68%)	18 (10.6%)	15 (8.77%)	0.409 [0.158;1.028]	
Tumor size					
T1	15 (4.27%)	2 (1.15%)	13 (7.34%)		
T2	78 (22.2%)	37 (21.3%)	41 (23.2%)	0.183 [0.025;0.734]	**<0.001**
T3	162 (46.2%)	73 (42.0%)	89 (50.3%)	0.201 [0.028;0.768]	
T4	96 (27.4%)	62 (35.6%)	34 (19.2%)	0.091 [0.013;0.361]	

Supplementary Table S2. Multivariate Cox regression for the GRG score and corresponding clinical features.

Characteristics	HR	lower .95	upper .95	p-value
Age	1.81	1.26	2.59	**0.001**
Tumor size	1.38	0.83	2.29	0.217
Lymph nodes	1.52	0.85	2.71	0.158
Metastasis	1.93	1.04	3.6	**0.038**
Stage	1.19	0.69	2.06	0.524
GRG score	1.57	1.11	2.23	**0.011**

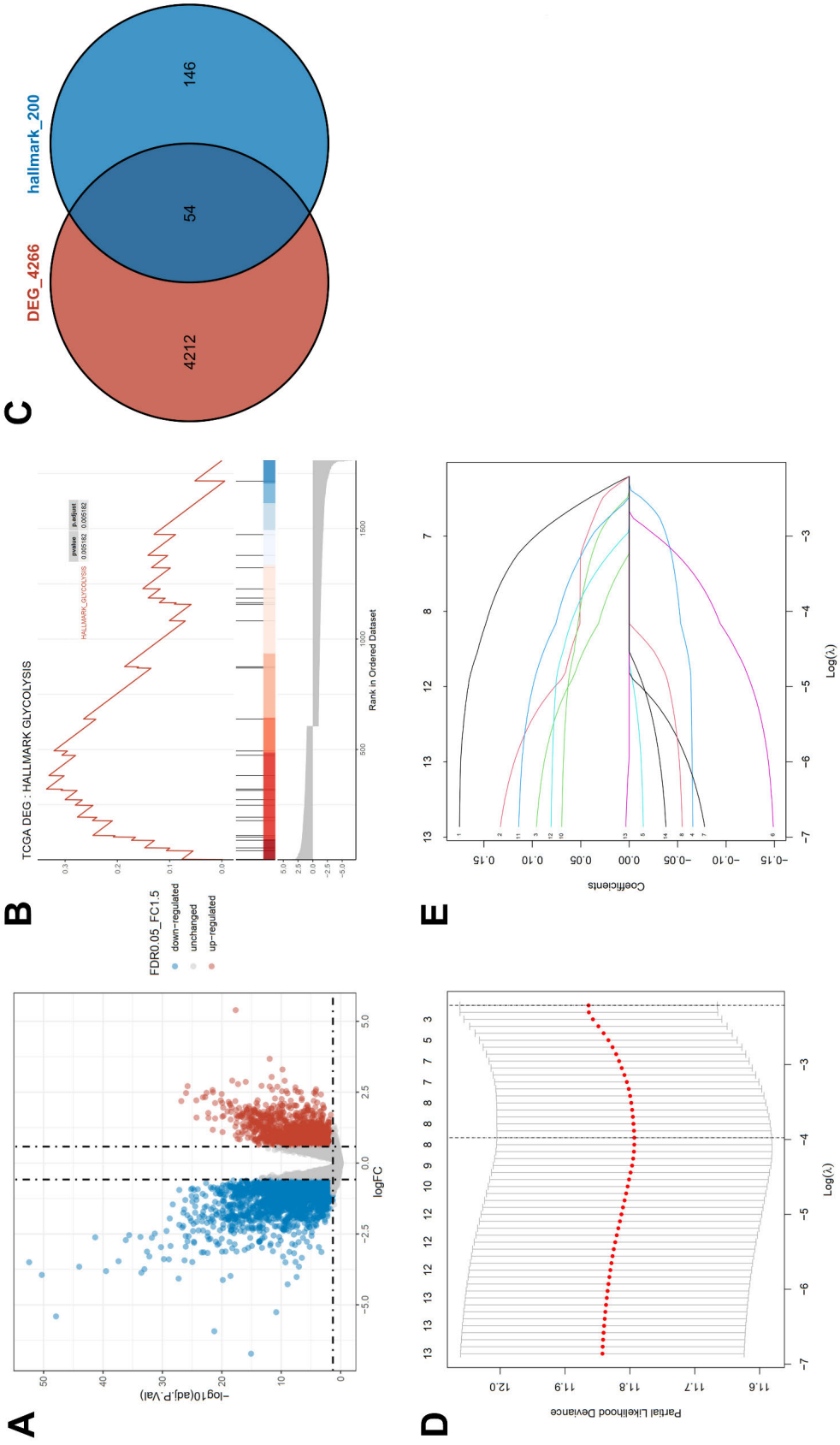

Supplementary Figure S1. Construction of the GRG score model in TCGA. A) Volcano plot presents the distribution of DEGs quantified between tumor and normal group with threshold of |log2 Fold change| > 1.5 and P < 0.05 in TCGA database. B)GSEA analysis was performed on HALLMARK_GLYCOLYSIS gene sets in gastric cancer DEGs. C) Venn diagram shows the intersection of glycolytic-related genes with GC differential genes in the TCGA dataset. D) LASSO coefficient profile plots of the GRG score model. Cross-validation to determine the optimal penalty parameter λ. E) Penalty plot for the LASSO regression for the GRGs with error bars denoting the standard errors.

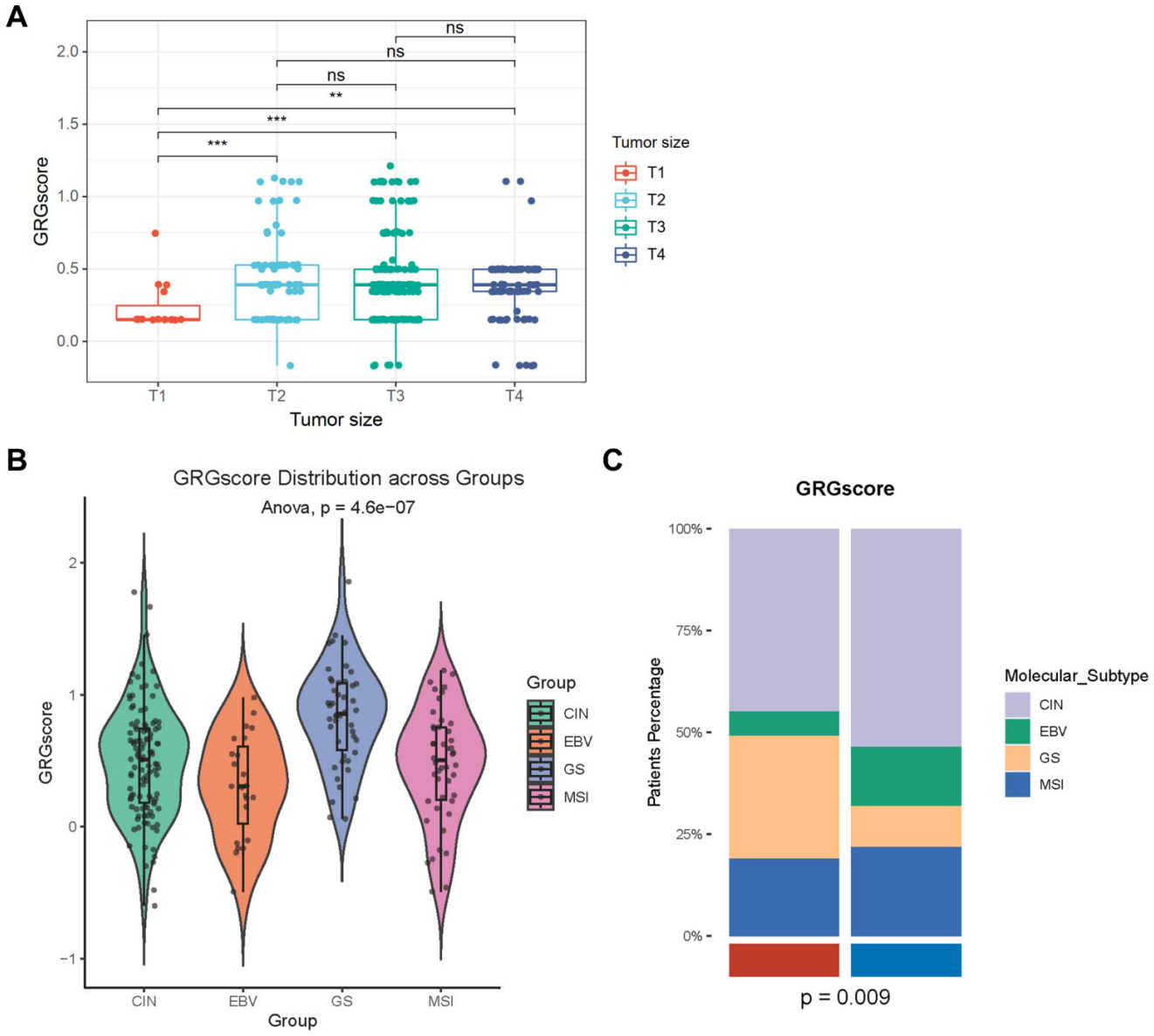

Supplementary Figure S2. Distribution of GRG scores in clinical patients with different tumor size and subtype. A) Boxplot showing the distribution of GRG scores across different tumor sizes (T1–T4) in TCGA-STAD samples. B) Violin plot illustrating the GRG score distribution among the four molecular subtypes of gastric cancer (CIN, EBV, GS, and MSI). C) Stacked bar plot comparing the proportion of high and low GRG score patients across molecular subtypes. Error bars indicate mean±SD. *p<0.05, **p<0.01, ***p<0.001

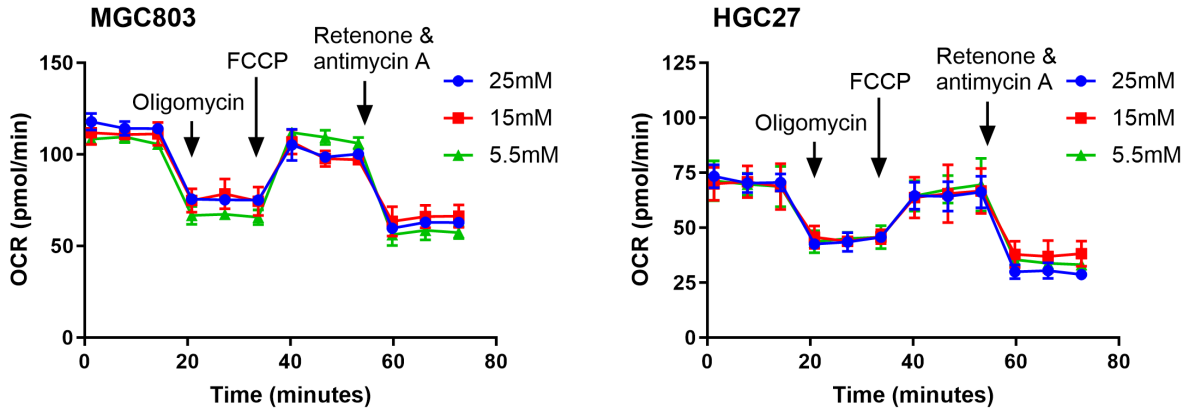

Supplementary Figure S3. Changes in oxygen consumption rate (OCR) of gastric tumor cells under different glucose concentrations.

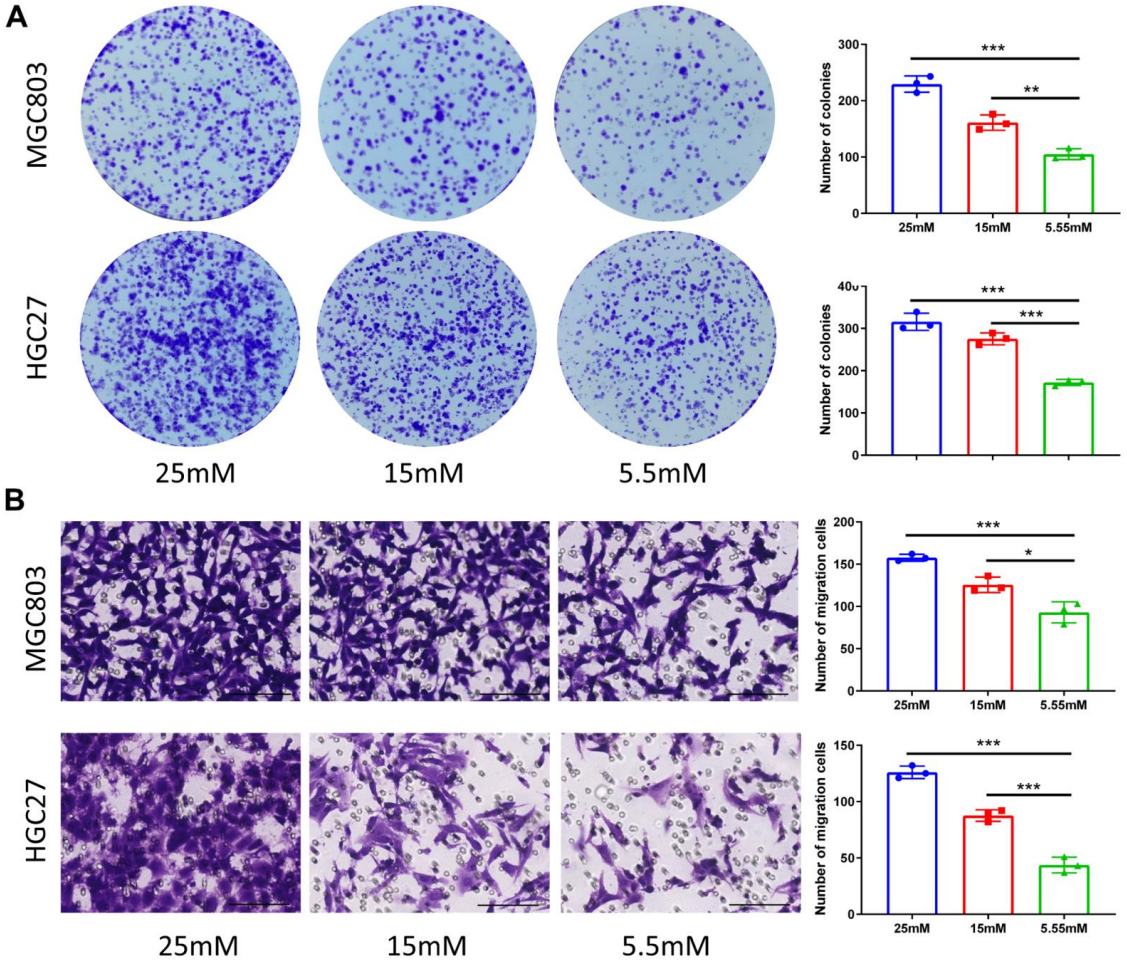

Supplementary Figure S4. Culture with different glucose concentration can affect the stem-related features of gastric cancer cells. A) The colony-formation ability of MGC803 and HGC27 cultured with different glucose concentrations was detected. B) The migration ability of MGC803 and HGC27 cultured with different glucose concentrations was detected. Scale bar, 100 μm. Error bars indicate mean±SD. *p<0.05, **p<0.01, ***p<0.001

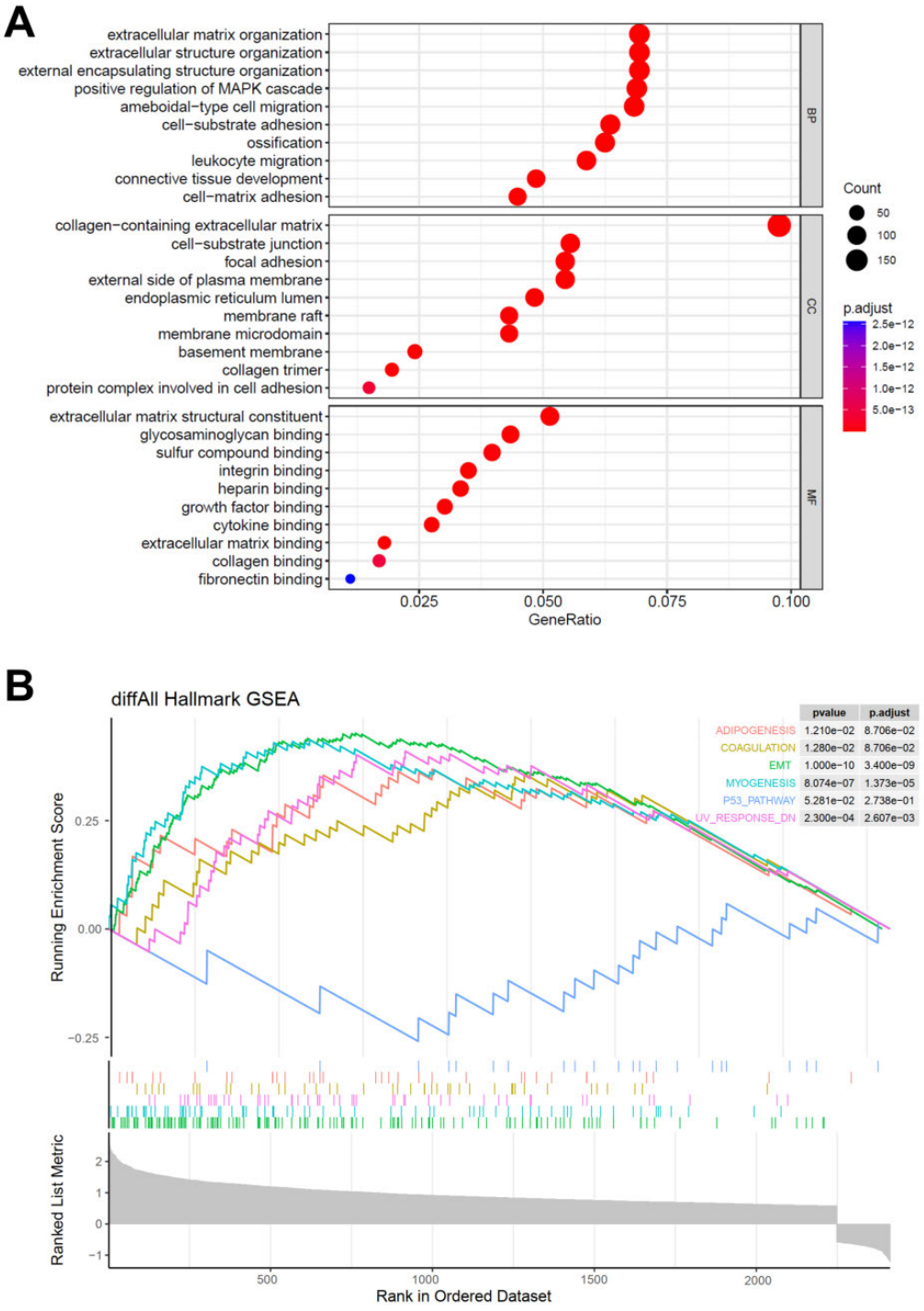

Supplementary Figure S5. High glycolysis can affect cell adhesion, cell migration and other functions, and affect EMT, P53 and other pathways. A) GO enrichment analysis of DEGs between high and low GRG score group. B) GSEA analysis was performed on HALLMARK gene sets in DEGs between high and low GRG score group.

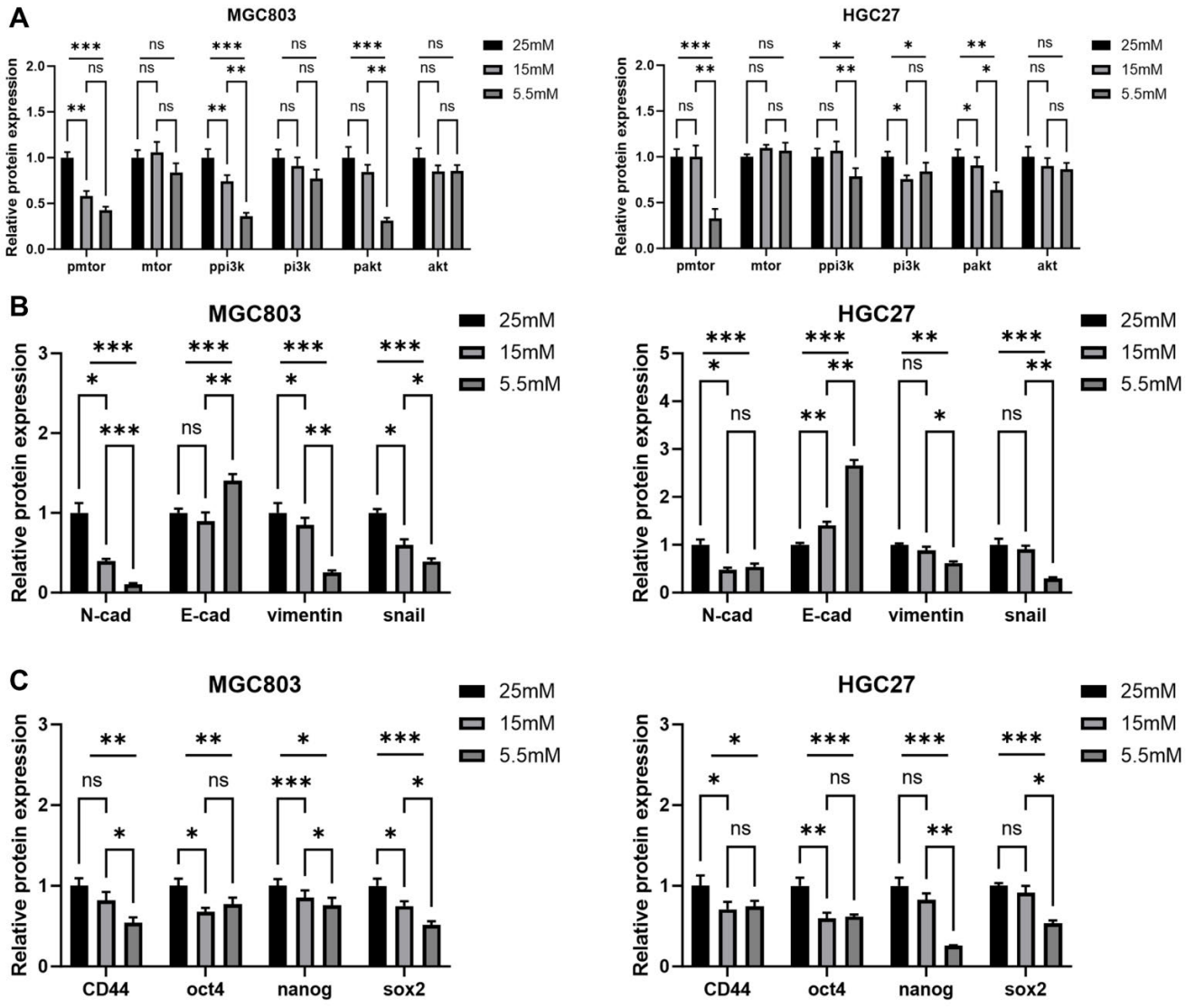

Supplementary Figure S6. Quantification of Western blot analyses in MGC803 and HGC27 gastric cancer cells cultured under different glucose concentrations. A) Expression of PI3K/AKT pathway proteins (pmTOR, mTOR, pPI3K, PI3K, pAKT, AKT). B) Expression of EMT-related markers (N-cadherin, E-cadherin, vimentin, snail). C) Expression of stemness markers (CD44, Oct4, Nanog, Sox2). Data are presented as means±SD. *p<0.05, **p<0.01, ***p<0.001; Abbreviation: ns-not significant